

# The oxidation states of copper and iron in mineral sulfides, and the oxides formed on initial exposure of chalcopyrite and bornite to air

Siew Wei Goh<sup>a</sup>, Alan N. Buckley<sup>a,\*</sup>, Robert N. Lamb<sup>a</sup>,  
Richard A. Rosenberg<sup>b</sup>, Damian Moran<sup>c</sup>

<sup>a</sup> *Surface Science and Technology, School of Chemistry, The University of New South Wales, Sydney, NSW 2052, Australia*

<sup>b</sup> *X-ray Operations and Research, Advanced Photon Source, Argonne National Laboratory, Argonne, IL 60439, USA*

<sup>c</sup> *School of Chemistry, The University of Sydney, Sydney, NSW 2006, Australia*

Received 1 November 2005; accepted in revised form 7 February 2006

## Abstract

Metal L<sub>2,3</sub>, sulfur K and oxygen K near-edge X-ray absorption fine structure (NEXAFS) spectra for chalcopyrite, bornite, chalcocite, covellite, pyrrhotite and pyrite have been determined from single-piece natural mineral specimens in order to assess claims that chalcopyrite should be regarded as Cu<sup>I</sup>Fe<sup>II</sup>S<sub>2</sub> rather than Cu<sup>I</sup>Fe<sup>III</sup>S<sub>2</sub>, and that copper oxide species are the principal initial oxidation products on chalcopyrite and bornite exposed to air. Spectra were obtained using both fluorescence and electron yields to obtain information representative of the bulk as well as the surface. Where appropriate, NEXAFS spectra have been interpreted by comparison with the densities of unfilled states and simulated spectra derived from ab initio calculations using primarily the FEFF8 code and to a lesser extent WIEN2k. Metal 2p and S 2p photoelectron spectra excited by monochromatised Al K<sub>α</sub> X-rays were determined for each of the surfaces characterised by NEXAFS spectroscopy. The X-ray excited Cu LMM Auger spectrum was also determined for each copper-containing sulfide. FEFF8 calculations were able to simulate the experimental NEXAFS spectra quite well in most cases. For covellite and chalcocite, it was found that FEFF8 did not provide a good simulation of the Cu L<sub>3</sub>-edge spectra, but WIEN2k simulations were in close agreement with the experimental spectra. Largely on the basis of these simulations, it was concluded that there was no convincing evidence for chalcopyrite to be represented as Cu<sup>II</sup>Fe<sup>II</sup>S<sub>2</sub>, and no strong argument for some of the Cu in either bornite or covellite to be regarded as Cu(II). The ab initio calculations for chalcopyrite and bornite indicated that the density of Cu d-states immediately above the Fermi level was sufficient to account for the Cu L<sub>3</sub>-edge absorption spectrum, however these incompletely filled Cu d-states should not be interpreted as indicating some Cu(II) in the sulfide structure. It was also concluded that the X-ray absorption spectra were quite consistent with the initial oxidation products on chalcopyrite and bornite surfaces being iron oxide species, and inconsistent with the concomitant formation of copper–oxygen species.

© 2006 Elsevier Inc. All rights reserved.

## 1. Introduction

Although caution should be exercised in assigning formal oxidation states to the constituent elements in transition metal chalcogenides of high conductivity, it is generally accepted that the oxidation state of copper in all sulfide minerals is nominally Cu(I), i.e., Cu with a

ground state configuration that is predominantly d<sup>10</sup> but including a small amount of d<sup>9</sup> character. That proposition was first put forward on the basis of stereochemistry, magnetic properties, and, for the Cu–Fe sulfides, Mössbauer spectra before relevant X-ray photoelectron spectroscopy (XPS) data had become available (Jellinek, 1972), but it was strengthened considerably on the basis of Cu 2p photoelectron spectra (Rupp and Weser, 1976; Nakai et al., 1978; Vaughan and Craig, 1978; Folmer and Jellinek, 1980; Folmer et al., 1988). Even the copper in CuS<sub>2</sub> is believed to be monovalent (van der Laan et al., 1992; Ueda

\* Corresponding author. Fax: +61 2 9662 1697.

E-mail address: [a.buckley@unsw.edu.au](mailto:a.buckley@unsw.edu.au) (A.N. Buckley).

et al., 2002). It is now widely considered that a principal Cu  $2p_{3/2}$  binding energy below but near the value for copper metal, 932.6 eV, the absence of a  $2p_{3/2}$  component above 933 eV, and the absence of excited final state satellites, indicate that a discernible concentration of Cu(II) is not present at unoxidised surfaces of the copper chalcogenides.

Until the report by Todd et al. (2003b), in which it is maintained that the copper in chalcopyrite is Cu(II), most NEXAFS spectra of the copper sulfides had been considered consistent with the Cu(I) formal oxidation state indicated by the Cu 2p photoelectron spectra and magnetic measurements. Even the Cu L-edge spectrum for chalcopyrite determined earlier by the same authors had been interpreted as arising from Cu(I) in the bulk mineral (Todd et al., 2000). A Cu  $L_3$  peak within the range 931.9–933.4 eV, rather than in the range 930.5–931.2 eV normally considered indicative of Cu(II), has usually been interpreted as confirmation that the copper in chalcopyrite, bornite, chalcocite and covellite is Cu(I) (van der Laan et al., 1992, 2002; Patrick et al., 1993, 1997), with the ground state being a mixture of Cu  $3d^{10}$ , Cu  $3d^{10}4s^1\underline{S}$  (where  $\underline{S}$  represents a hole in a sulfide 'ligand') and Cu  $3d^94s^1$  configurations. However, Todd et al. (2003b) have argued cogently that the Cu  $L_{2,3}$ -edge NEXAFS spectrum for chalcopyrite indicates the presence of all Cu(II) rather than Cu(I), and that the Cu L-edge spectrum for covellite is consistent with a significant fraction of the Cu being present as Cu(II). They arrived at this conclusion because the Cu L-edge spectra for chalcopyrite and covellite exhibited a strong peak near 932.4 eV, whereas the spectrum from the Cu in chalcocite, which is indisputably Cu(I), had its main absorption peak near 934.6 eV. Their conclusion for chalcopyrite appeared to be supported by the corresponding Fe  $L_3$ -edge NEXAFS spectrum which had an absorption peak at an energy similar to that for mackinawite ( $\text{FeS}_{1-x}$ ), and which they argued revealed the presence of Fe(II) rather than Fe(III). More recently, Mikhlin et al. (2005) have also argued that the total electron yield (TEY) Fe  $L_{2,3}$ -edge spectrum of chalcopyrite indicates predominantly Fe(II). Furthermore, they agreed with the conclusion of Todd et al. (2000) that the oxides present on the surface of air-exposed bornite are mostly those of copper rather than iron. Todd et al. (2003b) had also concluded that Cu oxides were included in the products formed on air-oxidised chalcopyrite. These findings appear to be inconsistent with XPS studies which have shown that Fe–oxygen species but not Cu–oxygen species are formed initially on exposure of Cu–Fe sulfides to air under ambient conditions (Brion, 1980; Buckley and Woods, 1983, 1984).

Of some concern in the work by Todd et al. (2003b) was the use of argon ion sputtering to remove any oxidised surface phase so that TEY absorption spectra would be representative of the bulk, but they also presented absorption spectra from surfaces that were described as pristine and therefore may not have been sputtered. When determining Cu or Fe L-edge spectra to obtain bulk information on sulfide minerals by monitoring only the TEY, it is important

to avoid oxidation products at the surface as the TEY analysis depth is expected to be less than 15 nm (Frazer et al., 2003). This is particularly pertinent for Cu(II) oxidation products, as the absorption intensity (transition probability) for Cu(II) has been estimated (Patrick et al., 1997) to be approximately 25 times that of Cu(I) because of the greater availability of d-like unfilled states in the nominally  $d^9$  system compared with the  $d^{10}$  configuration. When determining bulk properties from NEXAFS spectra by monitoring the fluorescence yield (FY), the presence of oxidised species at the surface is less important because of the several hundred nm analysis depth for FY.

Todd et al. (2003b) tacitly assumed that covellite contained both Cu(I) and Cu(II), but they did not provide an explanation for the apparent absence of evidence for Cu(II) in the Cu 2p photoelectron spectra for unoxidised covellite and chalcopyrite (e.g., Folmer and Jelinek, 1980; Buckley and Woods, 1984; Gebhardt et al., 1986). Also, mackinawite, the Fe(II) reference sulfide studied by Todd et al. (2003b), is known to be unstable in air (Boursiquot et al., 2001). Nevertheless, the NEXAFS spectra reported by Todd et al. (2003b) were of high quality in terms of both signal-to-noise and resolution, and hence the conclusions demand serious consideration. If the presence of Cu(II) in chalcopyrite and covellite were to be substantiated, then clearly the interpretation of the photoelectron spectra for copper sulfides would have to be re-examined, and the overall understanding of many of the sulfide minerals re-evaluated. Because of the importance of the Cu and Fe L-edge NEXAFS spectra for chalcopyrite in this regard, these spectra and the metal  $L_{2,3}$ -edge spectra for chalcocite, covellite, bornite, pyrite and pyrrhotite have been determined from single-piece mineral specimens not subjected to argon ion sputtering but by using FY/TFY to obtain information representative of the bulk. O K-edge and S K-edge NEXAFS spectra have also been determined, the latter in order to obtain complementary information on the involvement of sulfur p-states in the conduction band. Where appropriate, NEXAFS spectra have been interpreted by comparison with the density of unfilled states and simulated spectra calculated by means of the FEFF8 or WIEN2k codes. Metal 2p and S 2p photoelectron spectra, and metal LMM Auger electron spectra, excited by monochromatised Al  $K_\alpha$  X-rays were determined for each of the surfaces characterised by NEXAFS spectroscopy.

## 2. Experimental and computational details

Single pieces of mineral of approximate size  $6 \times 5 \times 0.5$  mm cut from large natural specimens were mounted using screws or conducting double-sided adhesive tape for NEXAFS spectroscopy and XPS. The pyrite, pyrrhotite ( $\text{Fe}_{0.89}\text{S}$ ), chalcocite, covellite, bornite and chalcopyrite samples were natural, massive specimens from Navajun (Spain), Mt Isa (Australia), Arizona (USA), Butte (USA), Kipuchi (Zaire) and Mt Lyell (Australia), respec-

tively. Microprobe analysis of the covellite specimen indicated that it was predominantly the single pure phase with a Cu:S ratio of 1.001:1, whereas the chalcocite specimen contained 20% djurleite ( $\text{Cu}_{1.96}\text{S}$ ). Before spectroscopic examination, the freshly abraded surface of each specimen was exposed to air under ambient conditions for at least a few minutes, and in a few cases when more extensive oxidation was required, for at least several hours.

NEXAFS spectroscopy on briefly air-exposed surfaces was carried out in a UHV end-station on the XOR 4-ID-C beam-line at the Advanced Photon Source, Argonne National Laboratory. The beam-line incorporated a spherical grating monochromator (SGM) equipped with several gratings to provide an energy range of 0.5–3.0 keV. With the 600 L/mm grating and 50  $\mu\text{m}$  slits used for the metal L-edge and O K-edge spectra, the monochromator resolution was 0.15 eV at the O K-edge and 0.5 eV at the Cu L-edge. With the 1200 L/mm grating and 25  $\mu\text{m}$  slits in place, the monochromator resolution was 1 eV at the S K-edge. X-ray absorption was monitored with a liquid-nitrogen cooled ultra-low energy germanium diode detector (FY), with a channel-plate detector behind retarding grids (TFY), and by means of drain current (TEY). No significant differences between the FY and TFY spectra were observed, and only the TFY spectra are shown. The synchrotron was operated in ‘continuous top-up’ mode. NEXAFS spectra from moderately oxidised surfaces were obtained on BL24A at the NSRRC, Taiwan, using either the 1600 L/mm or 800 L/mm grating in the SGM. The NEXAFS spectra were determined in TEY and TFY modes, the latter by means of a multichannel plate partial yield detector with the negative retard potential of sufficient voltage to allow for the presence of higher order radiation. For both sets of data, the photon flux incident on the specimen ( $I_0$ ) was monitored using a gold-coated mesh, and all spectra shown are normalised ( $I/I_0$ ). Copper metal and stainless steel were used for energy calibration at the Cu L-edge and Fe L-edge (932.6 and 706.8 eV for the TFY  $L_3$  absorption edge), respectively, and for the S K-edge, pyrite was used as a secondary calibrant relative to the edge and peak positions of 2472 and 2473 eV, respectively, for  $\text{S}_8$  (Petiau et al., 1988). The Fe L-edge calibration used in this work was in agreement with the spectra for Fe, Fe–Cr alloy and  $\text{Fe}_2\text{O}_3$  reported by Soriano et al. (1993) and for FeOH reported by Zheng et al. (2005). Calibration at the O K-edge was from the position of the leading absorption peak for FeOOH.

Conventional monochromatised Al  $K_\alpha$  XPS analyses were carried out on a VG ESCALAB 220-iXL spectrometer. An analyser pass energy of 20 eV and an electron take-off angle of 90° were used. Included in the binding energies used for calibration were 932.67 and 83.96 eV for Cu  $2p_{3/2}$  and Au  $4f_{7/2}$  from metallic copper and gold, respectively.

Density of states (DOS) calculations and NEXAFS spectra simulations were carried out primarily using version 8.20 (Ankudinov et al., 2002) of the FEFF program for both an unscreened and fully screened core

hole. The ab initio code includes a self-consistent field estimate of the Fermi level, as well as orbital occupancy and charge transfer. Potentials were calculated self consistently within a 0.5–0.7 nm radius cluster (about 35–100 atoms depending on the structure) around the absorbing atom with 15% overlap of the muffin-tin radii. Calculations using either the Hedin–Lundqvist exchange potential (primarily for the Fe  $L_3$ -edge and for the Cu  $L_3$ -edge of CuS and  $\text{Cu}_2\text{S}$ ) or the partially non-local Dirac–Fock/Hedin–Lundqvist (DFHL) potential (primarily for the S K-edge and the Cu  $L_3$ -edge) were carried out with full multiple scattering up to  $l=2$  with cluster radii of at least 1 nm, equivalent to about 300 atoms.

The input files for running FEFF8 were generated by the program ATOMS via the graphical interface TkATOMS (Ravel, 2001). The crystallographic structure data used in the calculations for the sulfides were those reported by Hall and Stewart (1973) for chalcopyrite, Koto and Morimoto (1975) for bornite, Evans (1971, 1979) for chalcocite, Evans and Konnert (1976) for covellite, King and Prewitt (1979) for  $\text{CuS}_2$ , Bayliss (1977) for pyrite, Powell et al. (2004) for pyrrhotite, Skála and Cisarová (2005) for troilite and Yamaguchi and Wada (1973) as well as Pechharromán et al. (1995) for  $\text{Fe}_2\text{S}_3$ . In its standard version, FEFF8 allows only seven unique potential indices in addition to the absorbing atom, therefore atoms in some complicated structures such as low chalcocite, bornite and pyrrhotite had to be grouped. Calculations were also carried out for chalcocite, covellite, chalcopyrite and bornite using version 2k (Schwarz et al., 2002) of the code WIEN (Blaha et al., 1990) which is based on density functional theory. The structure of chalcopyrite is related to that of sphalerite ( $\text{ZnS}$ ) with the Zn sites replaced equally by Cu and Fe (Vaughan and Craig, 1978). The structure of bornite is more complex, consisting of a superstructure of sphalerite-type units, with metal atoms in only half the tetrahedral sites, and antiferroite-type units, with metal atoms in all tetrahedral sites (Koto and Morimoto, 1975).

### 3. Results and discussion

#### 3.1. FEFF8 calculation of electronic properties

To a large extent, the core electron binding energies estimated by the FEFF8 code are determined by the composition and solid state structure of the material under investigation and the initial (normally ground state) electronic configuration selected for the relevant atom. The calculated values of the other electronic properties are also influenced by the form of the exchange potential selected to best simulate the experimental NEXAFS spectrum when convergence has been achieved. The best form of the exchange potential for a particular element in a given class of material is often well established, hence it is pertinent to consider whether FEFF8 calculations are able to determine formal oxidation states without the need for experi-

mental NEXAFS spectra in each case. In principle, it should be possible for a formal oxidation state to be revealed by the relevant calculated orbital occupancy or core electron binding energy.

### 3.1.1. Fe core electron binding energies, transferred charge and orbital occupancy

The *l*-projected charge counts calculated for spectator (non-absorbing) Fe and S atoms, as well as the total charge on the Fe atom, in a number of Fe and Cu/Fe sulfides are listed in Table 1 together with values for Fe, FeO, Fe<sub>2</sub>O<sub>3</sub>, Fe<sub>3</sub>O<sub>4</sub>, FeOOH, FeCl<sub>2</sub> and FeCl<sub>3</sub>. The calculated d occupancy for absorbing Fe atoms, Fermi level and Fe 2p<sub>3/2</sub> binding energy are also listed. An excited initial atomic configuration for iron of 3d<sup>7</sup>4s<sup>1</sup> rather than the ground state 3d<sup>6</sup>4s<sup>2</sup> was used for all iron-containing materials, as the latter configuration resulted in the charge on the sulfur (but not oxygen) atoms being slightly positive (Table 2), a condition that was considered untenable. It is evident from Table 1 that the non-absorbing Fe d occupancy is significantly greater than 6 for all the materials for which calculations were carried out, including those with Fe(III) formal oxidation state. The larger than expected charge count is most probably due to overestimation of s–p–d hybridisation. It is not an artefact of the use of the excited initial atomic configuration for iron, as it is clear from Table 2 that the d occupancy values were also greater than 6 for the ground state atomic configuration. It is also not an artefact of self-consistent field calculations that allowed *l* = 2 for S atoms; limiting the calculations to *l* = 1 resulted in a greater positive charge on the S atoms. The Fe d charge counts were not significantly influenced by different muffin-tin radii and overlap, different exchange potentials, or increased cluster size. The absorbing Fe atom d occupancies (Table 1) are, not surprisingly, approximately 1.1

greater than the spectator Fe atom d occupancies and hence provide similar information. These observations indicate that the absolute values of Fe d occupancy calculated by FEFF8 are probably not meaningful, although they may indicate a contribution from a d<sup>*n*+1</sup> final state. Furthermore, it can also be seen that the d charge counts are not markedly different for Fe(II) and Fe(III) in compounds with the same anion, such as oxides, suggesting that the difference in formal oxidation state may only correspond to a subtle difference in d occupancy. Indeed, the charge count for the octahedral Fe(III) in Fe<sub>2</sub>S<sub>3</sub> is comparable with the values for both pyrite and chalcopyrite, indicating that differentiation of Fe(II) from Fe(III) on this basis is unlikely to be possible. Nevertheless, it is interesting to note that the value for bornite is the highest of the sulfides under consideration, principally because of a lower than expected Cu charge count. Since the Fe d charge counts are observed to be similar for Fe(II) and Fe(III) in compounds with the same anion, it follows that the charge transferred from the Fe atoms to the anions is also unable to discriminate between the Fe formal oxidation states.

Unfortunately, neither the calculated total charge on the Fe atoms nor the calculated Fe 2p<sub>3/2</sub> binding energy appears to be a reliable indicator of formal oxidation state either. It can be seen from Table 1 that the total charge on the Fe atoms is essentially the same for Fe<sub>2</sub>S<sub>3</sub> as for pyrrhotite and troilite, and that the calculated Fe 2p binding energies for the sulfides are all within a 0.3 eV range. When the ground state configuration for Fe was used, most of the calculated Fe 2p binding energies and absorption energies were typically ~1 eV higher than when the excited atomic configuration for Fe was used. In the latter case, the calculated absorption energies were surprisingly close to the experimentally determined values.

Table 1

Fe and S or O *l*-projected charge counts for spectator Fe and S or O atoms, d counts for absorbing Fe atoms, Fermi level and Fe 2p<sub>3/2</sub> binding energy calculated by FEFF8 with Fe 3d<sup>7</sup>4s<sup>1</sup> initial state configuration

Material	Site	Spectator						Abs Fe d	<i>E<sub>F</sub></i> (eV)	Fe 2p <sub>3/2</sub> calc (eV)
		Fe s	Fe p	Fe d	ΣFe	S/O s	S/O p			
Fe		0.62	0.75	6.62	8.00				−9.76	709.6
FeO		0.38	0.54	6.79	7.71	1.85	4.44	7.91	−6.52	708.1
Fe <sub>2</sub> O <sub>3</sub>		0.42	0.62	6.58	7.62	1.85	4.41	7.66	−7.15	707.9
Fe <sub>3</sub> O <sub>4</sub>	Fe <sup>II</sup>	0.40	0.58	6.74	7.72	1.84	4.40	7.84	−6.68	708.0
	Fe <sup>III</sup>	0.46	0.64	6.58	7.68			7.73	−6.79	707.8
	Fe <sup>III</sup>	0.41	0.62	6.63	7.66	1.85	4.40	7.79	−6.67	708.0
FeOOH		0.43	0.63	6.60	7.66	1.84	4.38	7.63	−6.75	707.8
						1.87	4.42			
FeCl <sub>2</sub>		0.41	0.52	6.82	7.75				−5.92	707.5
FeCl <sub>3</sub>		0.42	0.57	6.72	7.71				−6.43	707.6
Fe <sub>1−<i>x</i></sub> S		0.46	0.62	6.85	7.93	1.84	3.99	0.36	−6.55	707.9
FeS		0.45	0.60	6.81	7.86	1.84	3.94	0.36	−6.89	708.0
Fe <sub>2</sub> S <sub>3</sub>	Fe <sup>oct</sup>	0.48	0.62	6.77	7.87	1.84	3.92	0.34	−6.97	707.7
	Fe <sup>tet</sup>	0.51	0.64	6.67	7.82				−6.97	707.9
FeS <sub>2</sub>		0.48	0.73	6.74	7.95	1.81	3.75	0.47	−6.15	708.0
Cu <sub>5</sub> FeS <sub>4</sub>		0.49	0.63	6.89	8.01	1.83	3.97	0.40	−6.29	707.9
CuFeS <sub>2</sub>		0.52	0.63	6.74	7.89	1.83	3.97	0.36	−6.78	707.8

Table 2  
Fe and S or O *l*-projected charge counts for spectator Fe and S or O atoms, Fermi level and Fe 2p<sub>3/2</sub> binding energy calculated by FEFF8 with Fe 3d<sup>6</sup>4s<sup>2</sup> initial state configuration

Material	Site	Fe s	Fe p	Fe d	ΣFe	S/O s	S/O p	S d	E <sub>F</sub> (eV)	Fe 2p <sub>3/2</sub> calc (eV)
Fe		0.63	0.77	6.59	8.00				−12.14	710.9
FeO		0.42	0.61	6.82	7.85	1.82	4.33		−8.04	709.2
Fe <sub>2</sub> O <sub>3</sub>		0.47	0.72	6.62	7.80	1.83	4.31		−8.70	709.0
Fe <sub>3</sub> O <sub>4</sub>	Fe <sup>II</sup>	0.43	0.65	6.72	7.80	1.83	4.30		−8.30	709.0
	Fe <sup>III</sup>	0.51	0.75	6.65	7.90	1.83	4.30			708.8
	Fe <sup>III</sup>	0.45	0.72	6.63	7.80					709.1
FeCl <sub>2</sub>		0.47	0.62	6.90	7.99	1.95	4.93	6.13	−6.40	708.6
FeCl <sub>3</sub>		0.49	0.70	6.83	8.02	1.95	4.92	0.13	−7.14	708.7
Fe <sub>1−x</sub> S		0.51	0.70	6.83	8.04	1.82	3.79	0.29	−8.21	709.0
FeS		0.50	0.69	6.88	8.07	1.82	3.79	0.31	−7.99	709.0
Fe <sub>2</sub> S <sub>3</sub>	Fe <sup>oct</sup>	0.54	0.72	6.83	8.09	1.82	3.80	0.30	−8.07	708.8
	Fe <sup>tet</sup>	0.60	0.74	6.79	8.13	1.83	3.80	0.30	−8.08	709.0
FeS <sub>2</sub>		0.56	0.88	6.87	8.30	1.79	3.64	0.42	−7.30	709.0
Cu <sub>5</sub> FeS <sub>4</sub>		0.59	0.79	7.08	8.46	1.82	3.93	0.39	−6.63	709.0
CuFeS <sub>2</sub>		0.61	0.76	6.86	8.23	1.82	3.89	0.33	−7.52	708.9

It will become evident from the calculations discussed below that neither an unreasonably large metal d count nor a positive charge on the sulfur atoms was observed for the copper sulfides. In the present investigation, a larger than expected metal d charge count and a positive charge on the sulfur atoms in the lattice have been observed for Fe, Co and Ni sulfides but not for Ti, Cr, Cu, Zn or Pb sulfides. It will also become evident that although the transferred charge calculated by FEFF8 does not appear to be able to differentiate Fe formal oxidation states, the simulated spectra can be used to assign the absorption peaks in the NEXAFS spectra. The simulated Fe L-edge spectra referred to in Section 3.2 were calculated with an unscreened core hole, as this arrangement provided an initial absorption peak intensity closer to that observed than did a screened core hole.

### 3.1.2. Cu core electron binding energies, transferred charge and orbital occupancy

Calculations were carried out with the usual 3d<sup>10</sup>4s<sup>1</sup> initial configuration for Cu. The *l*-projected charge counts calculated for spectator Cu and S atoms in several Cu and Cu/Fe sulfides are listed in Table 3, together with the

calculated Fermi level and Cu 2p<sub>3/2</sub> binding energy. Values for Cu, Cu<sub>2</sub>O, CuO, CuCl and CuCl<sub>2</sub> are also listed in Table 3 for comparison. It can be seen that the d-counts for both oxides are quite similar, as are the values for both chlorides, and hence the d-count is not a good indicator of formal oxidation state. By contrast the total charge on the Cu atoms in CuO and CuCl<sub>2</sub> is lower than for Cu<sub>2</sub>O, CuCl and the copper sulfides. In fact the total charge for each of the Cu sulfides, Cu/Fe sulfides and Cu(I) oxide or chloride is at least 10.9, compared with less than 10.9 for Cu(II) oxide or chloride. Nevertheless, the difference is not sufficiently clear to obviate the need for experimental NEXAFS spectra. As in the case of Fe, the estimated core electron binding energies do not provide a basis for differentiating the formal oxidation states of Cu.

Most of the simulated Cu L-edge spectra referred to in Section 3.3 were calculated with the DFHL exchange potential and an unscreened core hole to better reproduce the observed intensity of the first absorption peak. The absolute energies of the calculated and experimental Cu L-edge spectra aligned closely for the Cu/Fe sulfides and for CuS<sub>2</sub>, but not for chalcocite or covellite.

Table 3  
Cu and S or O *l*-projected charge counts for spectator Cu and S or O atoms, Fermi level and Cu 2p<sub>3/2</sub> binding energy calculated by FEFF8 with Fe 3d<sup>7</sup>4s<sup>1</sup> ground state configuration for the Cu/Fe sulfides, and binding energy measured by XPS

Material	Site	Cu s	Cu p	Cu d	ΣCu	S/O s	S/O p	S d	E <sub>F</sub> (eV)	Cu 2p <sub>3/2</sub> calc (eV)	Cu 2p <sub>3/2</sub> exp (eV)
Cu		0.66	0.61	9.73	11.00				−8.33	932.8	932.6
CuO		0.49	0.58	9.70	10.77	1.87	4.37		−7.85	931.8	933.8
Cu <sub>2</sub> O		0.60	0.58	9.74	10.92	1.88	4.27		−6.28	931.8	932.6
CuCl		0.52	0.57	9.90	10.99				−4.32	931.5	
CuCl <sub>2</sub>		0.46	0.51	9.91	10.88				−6.92	931.5	
Cu <sub>2</sub> S		0.59	0.62	9.77	10.98	1.83	3.86	0.34	−6.18	931.9	932.4
CuS	1	0.59	0.65	9.77	11.01	1.81	3.98	0.29	−6.19	931.8	931.95
	2	0.55	0.66	9.78	10.99	1.82	3.82	0.32		931.7	
CuS <sub>2</sub>		0.53	0.64	9.80	10.97	1.85	3.85	0.32	−7.01	931.6	
Cu <sub>5</sub> FeS <sub>4</sub>		0.53	0.59	9.79	10.91	1.83	3.92	0.30	−7.01	931.8	932.4
CuFeS <sub>2</sub>		0.54	0.61	9.75	10.90	1.83	3.89	0.28	−7.58	931.7	932.1

### 3.1.3. S core electron binding energies, transferred charge and orbital occupancy

Although S electronic environments were not the focus of this investigation, it is illuminating to examine the ability of FEFF8 to estimate S core electron binding energies in mineral sulfides. Calculated S  $2p_{3/2}$  and 1s binding energies and experimentally determined S  $2p_{3/2}$  values are listed in Table 4. It can be seen that for the two different S environments in CuS, the calculated binding energy difference is 0.45 eV (with the binding energy greater for the monosulfide) whereas the experimental difference is almost twice that value.

The calculated orbital occupancies for the Cu and Fe sulfides revealed only a 1% variation in the spectator S s-count, but a ~6% variation in the spectator S p-count. For example, the S p occupancy calculated for  $\text{FeS}_2$  was 3.75 whereas that for  $\text{Fe}_{1-x}\text{S}$  was 3.99 (Table 1). Thus, the S p-count appears to be somewhat more sensitive to chemical environment than the metal d-count.

## 3.2. Fe 2p photoelectron and NEXAFS spectra

### 3.2.1. Pyrite

Pyrite was included in this investigation primarily as a S K-edge energy reference but also as an Fe(II) sulfide reference. The Fe  $L_3$  leading absorption peak in the TEY spectrum reported by Todd et al. (2003a) for pyrite ground under nitrogen appeared to be split into a barely resolved doublet. It was argued that there should be no splitting of this peak for a pure pyrite surface (because the empty  $e_g$  orbitals are degenerate), and hence it was concluded that some Fe(III) must have been present at the pyrite surface either as an oxide or as a sulfide surface state. This explanation is not supported by the TEY and the TFY spectra shown in Figs. 1a and 2a as the leading absorption peak in the TFY spectrum is similar to that in the TEY spectrum obtained by Todd et al. (2003a). The higher energy compo-

Table 4  
S 1s and 2p binding energies calculated by FEFF8, and S 2p values determined experimentally

Material	Site	S 1s calc (eV)	S $2p_{3/2}$ calc (eV)	S $2p_{3/2}$ exp (eV)
$\text{FeS}_2$		2469.5	160.55	162.4
$\text{Fe}_{1-x}\text{S}$	Five-coordinate	2469.45	160.5	161.2
	Six-coordinate	2469.3	160.35	162.3 <sup>a</sup>
FeS		2469.1	160.2	
		2469.3	160.4	161.85 <sup>a</sup>
		2469.5	160.6	
$\text{Fe}_2\text{S}_3$		2469.2	160.3	
$\text{Cu}_2\text{S}$		2469.4	160.4	161.5
CuS	Monosulfide	2469.35	160.4	160.9
	Disulfide	2468.9	159.95	161.75
$\text{CuS}_2$		2468.7	159.8	
$\text{Cu}_5\text{FeS}_4$		2468.9	160.3	161.4
$\text{CuFeS}_2$		2469.3	160.4	
		2469.35	160.4	161.4

<sup>a</sup> Skinner et al. (2004).

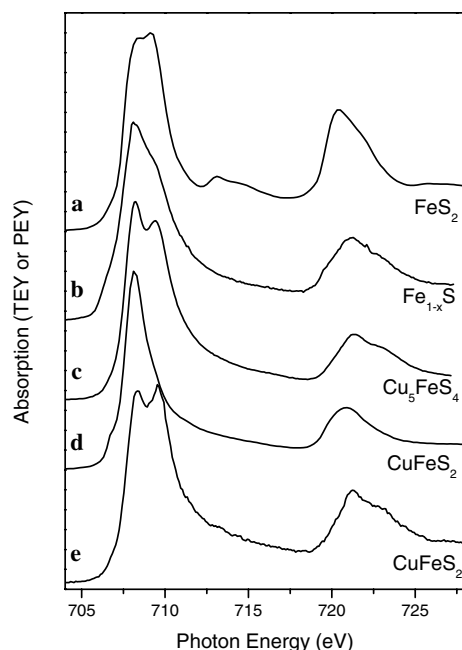


Fig. 1. TEY Fe  $L_{2,3}$ -edge NEXAFS spectrum for (a) pyrite; (b) pyrrhotite; (c) bornite; (d) chalcopyrite exposed briefly to air, and PEY spectrum for (e) chalcopyrite exposed to air for 2 days.

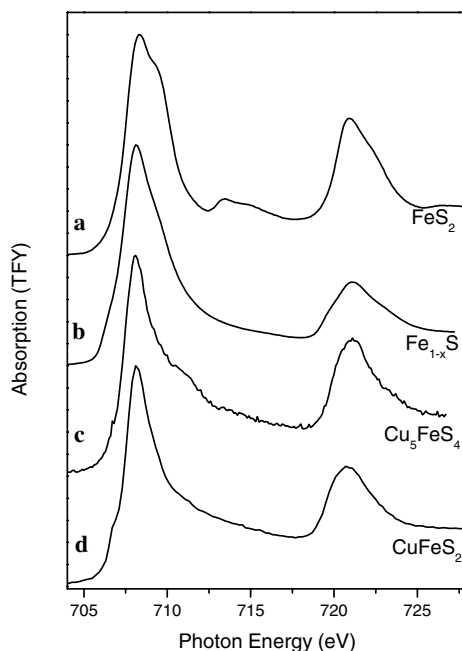


Fig. 2. TFY Fe  $L_{2,3}$ -edge NEXAFS spectrum for (a) pyrite; (b) pyrrhotite; (c) bornite; (d) chalcopyrite exposed briefly to air.

ment of the doublet-like structure in the TEY spectrum for the air-exposed single piece specimen was noticeably more intense than in the corresponding TFY spectrum suggesting that some oxidation of the surface had occurred. For both the TEY and TFY spectra, the apparent peak positions are at 708.3 and 709.3 eV, however the true splitting would be slightly greater than 1.0 eV, and the overall

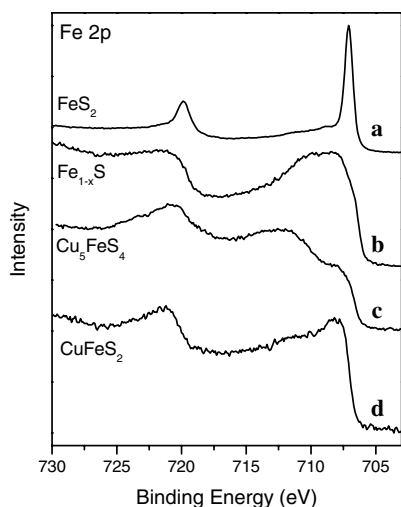


Fig. 3. Fe 2p photoelectron spectrum for the surface examined by XAS of (a) pyrite; (b) pyrrhotite; (c) bornite; (d) chalcopyrite.

$L_{3}$ -edge spectrum is more complex than a simple doublet. The Fe 2p photoelectron spectrum (Fig. 3a) confirmed that a low concentration of Fe(III) oxide was present at the surface of the specimen examined by XAS.

The Fe  $L_{2,3}$ -edge spectra obtained in this work and by Todd et al. (2003a) were qualitatively similar to the TEY spectra determined by Charnock et al. (1996) for pyrite ground with graphite, and by Suga et al. (1999) and Doyle et al. (2004) for a natural single crystal. The  $L_{3}$ -edge spectrum calculated by Charnock et al. (1996) based on the atomic multiplet approach was a reasonable simulation of the experimental spectrum, reproducing to some extent the poorly resolved doublet nature of the main peaks. The ground state electronic structure calculated by Eyert et al. (1998) based on density functional theory revealed a more pronounced doublet-like structure in the density of unfilled states between  $\sim 1.5$  and  $\sim 4$  eV. Notwithstanding

the less-than-perfect but quite acceptable agreement with the experimental spectrum, the FEFF8 simulation with  $3d^7 4s^1$  initial state configuration and unscreened core hole (Fig. 4a) also reveals that the  $L_{3}$ -edge doublet-like structure is intrinsic for pyrite, and not a result of the presence of Fe(III). The simulated spectrum agrees more closely with the TFY than the TEY spectrum as the calculation is for the bulk rather than the surface structure.

The Fe  $L_{2,3}$ -edge spectra for  $Fe_2O_3$  and FeOOH reported by Todd et al. (2003a) show an absorption peak with a minor component near 709 eV and a major component near 710.5 eV. The spectrum for  $Fe_2O_3$  reported by Soriano et al. (1993) showed the corresponding peaks near 708 and 709.8 eV, values closer to those obtained for FeOOH in the present investigation (707.9 and 709.4 eV) and by Zheng et al. (2005). Even accepting the absorption peak energies for the Fe  $L$ -edge data of Todd et al. (2003a), these observations for the Fe(III) species, and that for pyrite described above, indicate that absorption peaks in the energy ranges 707.5–709 and 709–710 eV do not necessarily imply the presence of Fe(II) and Fe(III), respectively.

### 3.2.2. Pyrrhotite

Pyrrhotite was investigated primarily as a reference for surface iron oxide species, but also as another predominantly Fe(II) sulfide reference. XPS studies have established that iron oxide and hydroxyoxide are formed rapidly, and before sulfur–oxygen species, at the surface of pyrrhotite exposed to the atmosphere (Buckley and Woods, 1985), unlike pyrite under similar conditions (Buckley and Woods, 1987). The Fe 2p photoelectron spectrum (Fig. 3b) of one of the briefly exposed surfaces examined by XAS in this work confirmed that moderate oxidation of the surface had occurred. Accordingly, a significant contribution from oxidised iron would be expected in even the FY Fe  $L$ -edge spectrum from a surface exposed to air for several minutes. The observed Fe  $L_{3}$  absorption

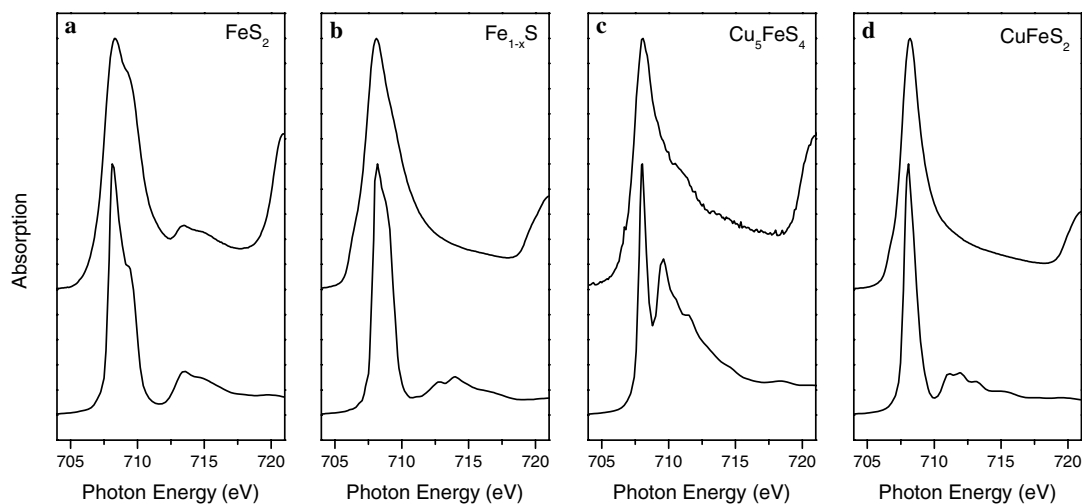


Fig. 4. TFY Fe  $L_{3}$ -edge NEXAFS spectrum (upper curve) and spectrum calculated using FEFF8 (lower curve) for (a) pyrite; (b) pyrrhotite; (c) bornite; (d) chalcopyrite.

peak obtained in TEY and TFY modes (Figs. 1b and 2b) was relatively broad, and appeared to consist of two main components, with the higher energy component slightly more intense in the TEY than in the TFY spectrum. The principal component and peak maximum was at 708.2 eV, and there was a less intense (but unresolved) component near 709 eV that would have arisen, at least in part, from iron oxide at the surface of the specimen. The shoulder due to a low intensity component near 706.8 eV was not a normalisation artefact arising from absorption by stainless steel in the beam-line. A shoulder due to a component near 706 eV (1.7 eV below the main peak) was also detected for natural pyrrhotites by Mikhlin and Tomashevich (2005), and Lawniczac-Jablonska et al. (1997) observed a shoulder near 707 eV for synthetic FeS.

The FEFF8 simulation for the Fe L-edge of pyrrhotite (Fig. 4b) indicates that the L<sub>3</sub> absorption peak consists of two principal components separated by about 0.7 eV. Thus, part of the absorption intensity observed in the 709–709.5 eV range would have been inherent to the pyrrhotite structure and some would have arisen from surface Fe oxide species.

### 3.2.3. Bornite

The Fe L<sub>3</sub> absorption peak in the TEY and TFY spectra for bornite exposed briefly to air (Figs. 1c and 2c) was split

into a clearly resolved doublet at 708.1 and 709.5 eV. The intensity of the component at 709.5 eV was more intense in the TEY spectrum than in the TFY spectrum, almost certainly because of the superposition at that energy of a component from Fe(III)-oxide present at the bornite surface. The presence of oxidised Fe at the surface exposed briefly to air was confirmed by the obvious peak near 712 eV in the Fe 2p photoelectron spectrum (Fig. 3c). The fact that the component at 708.1 eV in the corresponding TFY spectrum was more intense than that near 709.5 eV indicates that at least the former component is intrinsic to bornite. Mikhlin et al. (2005) reported TEY Fe L<sub>2,3</sub>-edge spectra for synthetic bornite that were similar to the spectrum in Fig. 1c. Their spectra for specimens abraded in vacuum and abraded in air were essentially the same.

Given that the formal oxidation state for copper in bornite is expected (from stoichiometric, magnetic and XPS considerations) to be Cu(I), then the iron oxidation state would be Fe(III). Even if it were argued that bornite should be viewed as Cu<sup>II</sup>Cu<sub>4</sub>Fe<sup>III</sup>S<sub>4</sub> rather than Cu<sup>I</sup><sub>5</sub>-Fe<sup>III</sup>S<sub>4</sub>, 20% of the copper with formal oxidation state Cu(II) would not be consistent with other spectroscopic measurements. Therefore, the component near 708 eV accounting for most of the intensity of the leading peak in the Fe L<sub>3</sub>-edge spectrum should not be

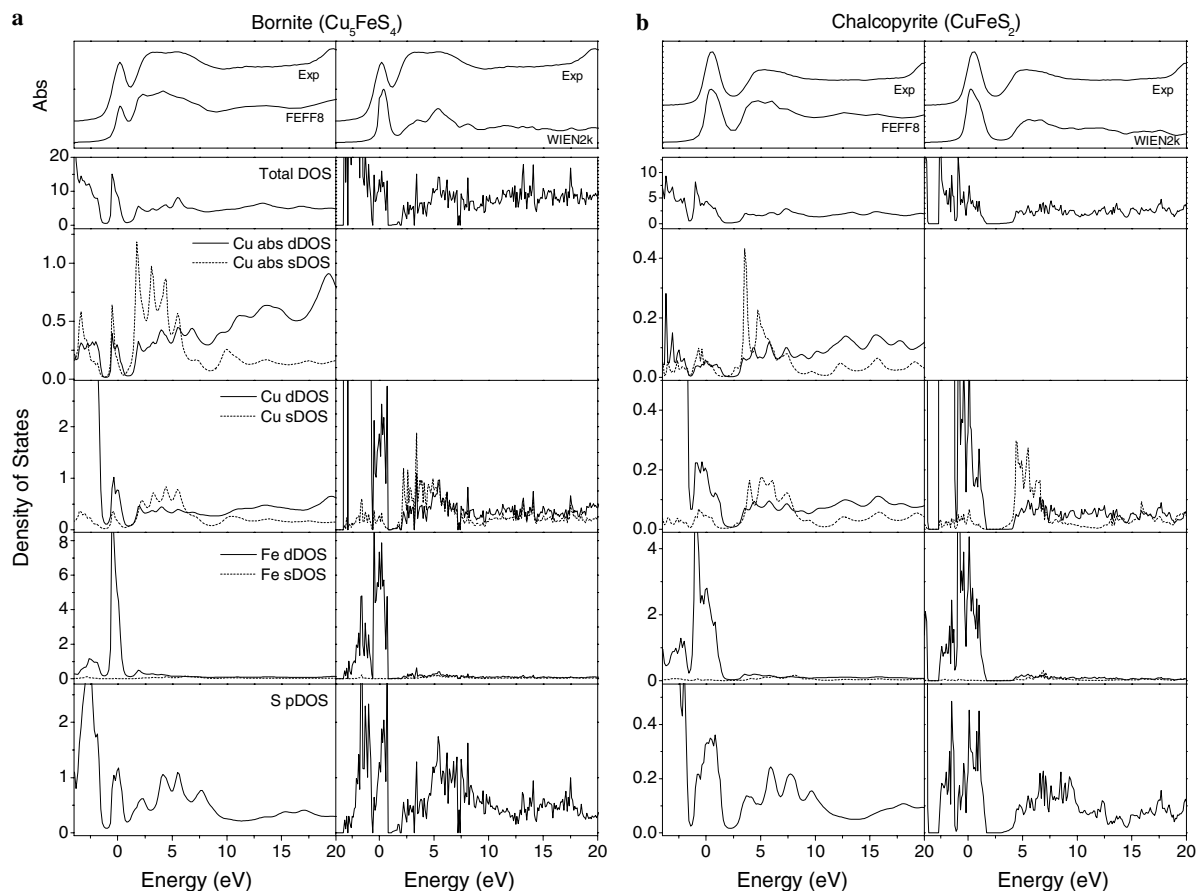


Fig. 5. TFY and simulated Cu L<sub>3</sub>-edge NEXAFS spectra, and density of states calculated by FEFF8 and WIEN2k for (a) bornite; (b) chalcopyrite.

viewed as being inconsistent with Fe(III), just as a component at 709.3 eV in the spectrum from pyrite should not be regarded as being inconsistent with Fe(II). Indeed any generalisation that an initial Fe L<sub>3</sub>-edge absorption peak significantly below 709 eV, without a component of comparable or greater intensity ~1 eV higher, is indicative of Fe(II) rather than Fe(III) is too simplistic.

The FEFF8-simulated Fe L<sub>3</sub>-edge spectrum for bornite is shown in Fig. 4c together with the corresponding TFY spectrum. The agreement between the simulated and experimental spectra appears to be quite good, in that both consist primarily of a single, intense absorption peak at a relatively low energy, as might be expected from the calculated Fermi level being situated ~0.8 eV below the upper limit of the main Fe d-DOS band (Fig. 5a). However, the experimental spectrum was perhaps broader than expected from the other sulfides studied. It should be noted that the simulated spectra in Fig. 4 are shown at the calculated absorption energies, and not artificially aligned with the experimental spectra.

Todd et al. (2000) claimed that bornite oxidised to a copper rather than an iron oxide, and that the absence of surface iron was confirmed by the Fe L-edge spectrum. The difference in the TEY and TFY spectra shown in Figs. 1c and 2c does not support the assertion that there is no evidence for the presence of an iron oxide in the Fe L-edge spectrum. Moreover, the TEY Fe L<sub>2,3</sub>-edge spectrum for bornite exposed to air for 2.5 h showed an even greater influence from a component near 709.5 eV than for brief exposure, confirming an increase in the concentration of iron (hydroxy)oxide at the surface.

### 3.2.4. Chalcopyrite

The Fe 2p photoelectron spectrum from the briefly air-exposed chalcopyrite specimen examined by XAS (Fig. 3d) confirmed the expected lower concentration of surface oxidation products relative to that for bornite (Fig. 3c). Previous XPS studies have established that the oxidation rate of chalcopyrite is significantly lower than that for bornite when exposed to air under ambient conditions (Buckley and Woods, 1983, 1984).

The TEY and TFY Fe L<sub>2,3</sub>-edge spectra for briefly air-exposed chalcopyrite (Figs. 1d and 2d) were essentially the same, with the leading resolved peak at 708.1 eV. The similarity of the TEY and TFY spectra was consistent with the less oxidised surface of chalcopyrite compared with that of the bornite. Apart from a very low intensity shoulder near 707 eV, the L-edge spectra were quite similar to the TEY spectrum obtained by Mikhlin et al. (2004, 2005), and qualitatively similar to that observed by Todd et al. (2003b), who reported the leading peak to be at 708.8 eV.

The FEFF8-simulated Fe L<sub>3</sub>-edge spectrum for chalcopyrite is shown in Fig. 4d. The agreement between the simulated and experimental spectra is quite good. Both consist essentially of a single, intense absorption peak at a relatively low energy, as might be expected from the calculated

Fermi level being situated ~1.6 eV below the upper limit of the Fe d-DOS (Fig. 5b).

As confirmed by the Fe L<sub>3</sub>-edge spectrum from bornite, a peak at 708.1 eV does not necessarily indicate that the iron in CuFeS<sub>2</sub> is Fe(II) as claimed by Todd et al. (2003b). Following the approach proposed by van Aken and Liebscher (2002), Mikhlin et al. (2005) also argued that the Fe in CuFeS<sub>2</sub> is predominantly Fe(II) because the L<sub>3</sub> absorption peak consisted largely of a single component at 707.8 eV, whereas they considered their TEY Fe L-edge spectrum for bornite resembled spectra for Fe(III) compounds because the component at 709.3 eV was more intense than the 707.8 eV component. However, it can be seen from Figs. 2c and d that the Fe L<sub>2,3</sub>-edge spectra for bornite and chalcopyrite are quite similar when the former is largely unaffected by a contribution from surface oxidation products.

## 3.3. Cu 2p photoelectron, Auger and NEXAFS spectra

### 3.3.1. Copper metal

Cu L-edge NEXAFS spectra from air-exposed Cu metal were determined periodically throughout the sulfide mineral data collection period to monitor the photon energy calibration and stability, and to serve as an energy reference for the absorption peaks from any Cu–O species present on the surface of the sulfides. For the latter purpose, it was first necessary to confirm the identity of the Cu–O species on the metal with XPS, and then compare the absorption energies with those for the bulk copper oxides used in some other studies.

The TEY and TFY Cu L<sub>2,3</sub>-edge NEXAFS spectra for copper metal, purposely exposed to air for several days to develop an oxidised surface layer, are shown in Figs. 6a and 7a, respectively. It can be seen that in the TEY spectrum, a low intensity peak at 931.3 eV, due to a very low concentration of Cu(II) oxide, was observed

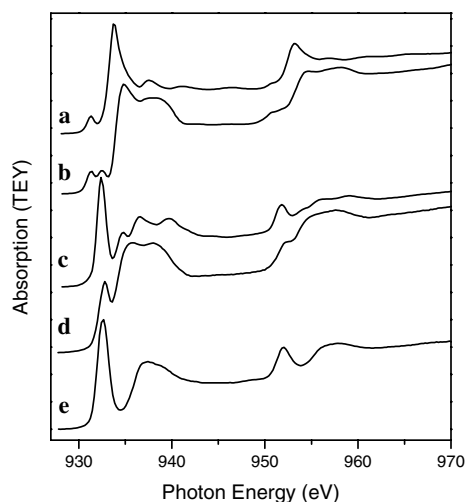


Fig. 6. TEY Cu L<sub>2,3</sub>-edge NEXAFS spectrum for air-exposed (a) copper metal; (b) chalcocite; (c) covellite; (d) bornite; (e) chalcopyrite.

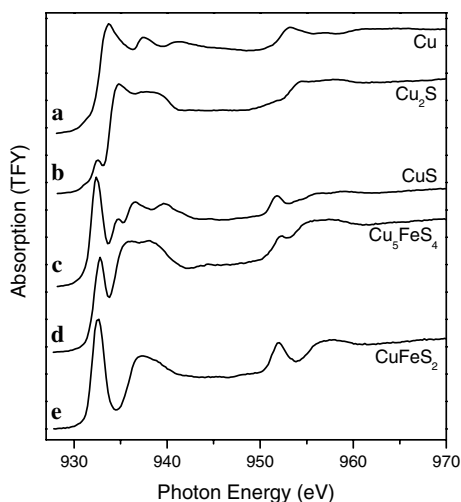


Fig. 7. TFY Cu  $L_{2,3}$ -edge NEXAFS spectrum for air-exposed (a) copper metal; (b) chalcocite; (c) covellite; (d) bornite; (e) chalcocopyrite.

before an intense absorption edge near 933 eV and peak at 933.7 eV indicative of Cu(I) oxide. As expected, the contribution from the oxides was barely evident in the TFY Cu L-edge spectrum (Fig. 7a) in which the main absorption edge was at 932.6 eV due to Cu metal. Any contribution from Cu metal in the TEY spectrum would not have been resolved from the Cu(I) oxide absorption. These assignments were confirmed with XPS. In the Cu 2p photoelectron spectrum and Cu LMM Auger spectrum from the air-exposed copper metal (Fig. 8a), the absence of excited final state satellite structure and the absence of a clear Cu 2p component shifted 1.1–1.2 eV to higher binding energy from that for Cu metal and  $\text{Cu}_2\text{O}$ , confirmed the absence of a significant concentration of a Cu(II)–oxygen species. In the same Auger spectrum, a Cu  $L_3M_{4,5}M_{4,5}$  peak at a kinetic energy of 916.3 eV was consistent with the presence of  $\text{Cu}_2\text{O}$ .

The absorption peak energy of 931.3 eV observed for the Cu(II)–oxygen species in the TEY spectrum was the same as that determined by Grioni et al. (1989) for CuO powder, and close to the value of 931.2 eV reported for tenorite (CuO) by van der Laan et al. (1992). It is also close to the energy of 931.4 eV assigned to CuO by Todd et al. (2003b), therefore the Cu L-edge absorption energies determined in the present investigation for the copper sulfides are directly comparable with those found previously.

### 3.3.2. Chalcocite

The TEY Cu  $L_{2,3}$ -edge spectrum for briefly air-exposed chalcocite (Fig. 6b) was similar to the TFY spectrum (Fig. 7b) apart from a small additional peak near 931.3 eV in the former arising from a Cu(II) surface oxidation product. Supporting evidence for no more than a low concentration of such a surface species can be seen in the Cu 2p photoelectron spectrum (Fig. 8b) from the same chalcocite specimen. A relatively weak peak near 932.4 eV was also evident in both the TEY and TFY spectra (Figs. 6b and 7b), and assignment of this peak, which was also observed by Grioni et al. (1989) and van der Laan et al. (1992) but not by Todd and Sherman (2003) or Todd et al. (2003b), is fundamental to the issues being addressed in this work. van der Laan et al. (1992) assigned the absorption peak that they observed at 932.1 eV as an integral part of the chalcocite absorption spectrum, rather than to a Cu(II)–sulfide species as did Todd et al. (2003b) for an absorption peak near 932.3 eV from covellite. It is conceivable that the peak at 932.4 eV could have arisen from Cu of formal oxidation state Cu(II) in the  $\text{Cu}_{1.96}\text{S}$  known to be present in the copper sulfide specimen, as it has been proposed that djurleite can be regarded as  $\text{Cu}^{\text{I}}_{62}\text{Cu}^{\text{II}}\text{S}_{32}$  (Goble, 1985). Alternatively, it could have arisen from Cu(I) in another minor copper sulfide phase such as CuS, for which the initial absorption peak is near 932.4 eV. In prin-

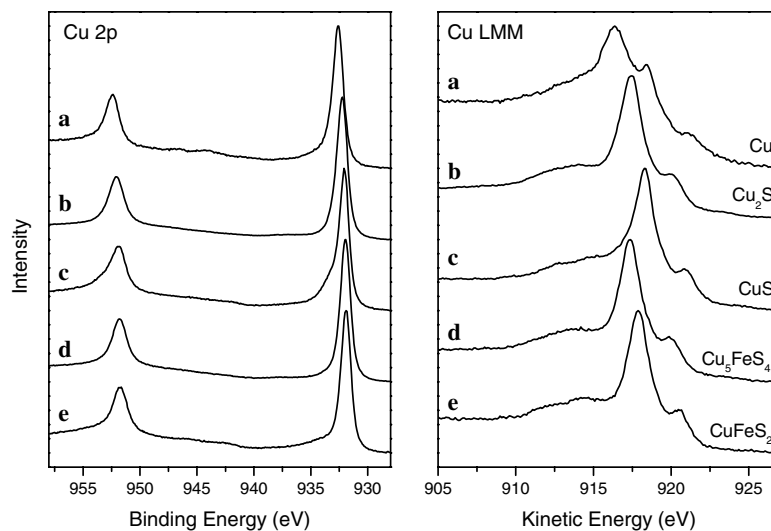


Fig. 8. Cu 2p photoelectron and Cu LMM Auger spectra for the surface examined by XAS of (a) copper metal; (b) chalcocite; (c) covellite; (d) bornite; (e) chalcocopyrite.

inciple, the peak could also have arisen from a non-sulfide and non-oxide impurity phase in the chalcocite, such as a copper halide, but no impurity element of sufficient concentration could be detected by XPS or electron microprobe. However, the WIEN2k calculations described below confirm that the 932.4 eV peak is indeed an integral part of the chalcocite spectrum.

The small peak at 932.4 eV was not reproduced in the chalcocite Cu L<sub>3</sub> spectrum simulated by means of the FEFF8 code, but apart from that peak, the form of the Cu L<sub>3</sub> spectrum was simulated reasonably well. As can be seen from Fig. 9a, when the sum of spectra simulated for all 24 Cu sites in chalcocite was shifted ~1.5 eV to higher energy, the agreement with the experimental spectrum was adequate. Nevertheless, it should be noted that the only other FEFF8-simulated Cu L-edge spectrum that would have to be shifted by more than ~0.2 eV to achieve alignment with the observed spectrum is that for CuS discussed below. The FEFF8 calculations suggest that the overall appearance of the spectrum for chalcocite is quite different from those for the other copper sulfides investigated largely because the Fermi level lies towards the end of a region of low, rather than within a region of moderately high, density of Cu d-states.

The WIEN2k code is better able than FEFF8 to simulate the Cu L<sub>3</sub>-edge spectrum for chalcocite (Fig. 9a). It seems that the WIEN2k simulation is more successful largely because of a better estimate of the Fermi level rather than a markedly different energy distribution of the density of states. However, in comparing the relative merits of FEFF8 and WIEN2k, it should be noted that ab initio calculations using WIEN2k can be significantly more time-consuming than those using FEFF8 for complex unit cells such as that for chalcocite. The WIEN2k calculations confirm that the peak at 932.4 eV is an integral part of the absorption spectrum from the chalcocite lattice, and that the peak at 932.4 eV arises because the Fermi level is

located near the upper limit of the Cu d-states. It does not arise from Cu s-states, as the density of Cu s-states immediately above the Fermi level is much lower than the density of d-states.

### 3.3.3. Covellite

The TEY and TFY Cu L<sub>2,3</sub>-edge spectra for covellite exposed briefly to air were essentially the same (Figs. 6c and 7c), apart from the leading absorption peak at 932.4 eV being slightly more intense in the former. These spectra were similar to the TEY spectra reported by Grioni et al. (1989) and van der Laan et al. (1992), in which the leading absorption peak energy was at 932.0 eV. Todd et al. (2003b) observed the main TEY absorption peak at 932.2 eV, but in addition, obtained an obvious shoulder near 931 eV consistent with a Cu(II)–oxygen species at the surface of their nearly pristine covellite. They interpreted the peak at 932.2 eV as arising from Cu(II) bonded to sulfur, and the peak near 934.7 eV as arising from Cu(I) in the sulfide lattice, superficially consistent with their assertion that CuS contains both Cu(I) and Cu(II). Although only 1/3rd of the Cu in CuS would be Cu(II) if it were assumed to be Cu<sup>I</sup><sub>2</sub>S·Cu<sup>II</sup>S<sub>2</sub>, as noted above the absorption intensity for Cu(II) is 25 times that for Cu(I) consequently an absorption peak arising from the Cu(II) would be almost an order of magnitude more intense than that from the Cu(I).

The Cu 2p (Fig. 8c) and S 2p photoelectron spectra from the mineral specimen examined by XAS in the present investigation were consistent with the covellite crystal structure and with a Cu(I) formal oxidation state, notwithstanding broad (presumably energy-loss) features on the high binding energy side of both the Cu 2p and S 2p peaks. No excited final state satellites that could have arisen from Cu(II) were evident in the Cu 2p spectrum, in agreement with previous investigations (e.g., Gebhardt et al., 1986; Perry and Taylor, 1986). The Cu 2p and O 1s photoelec-

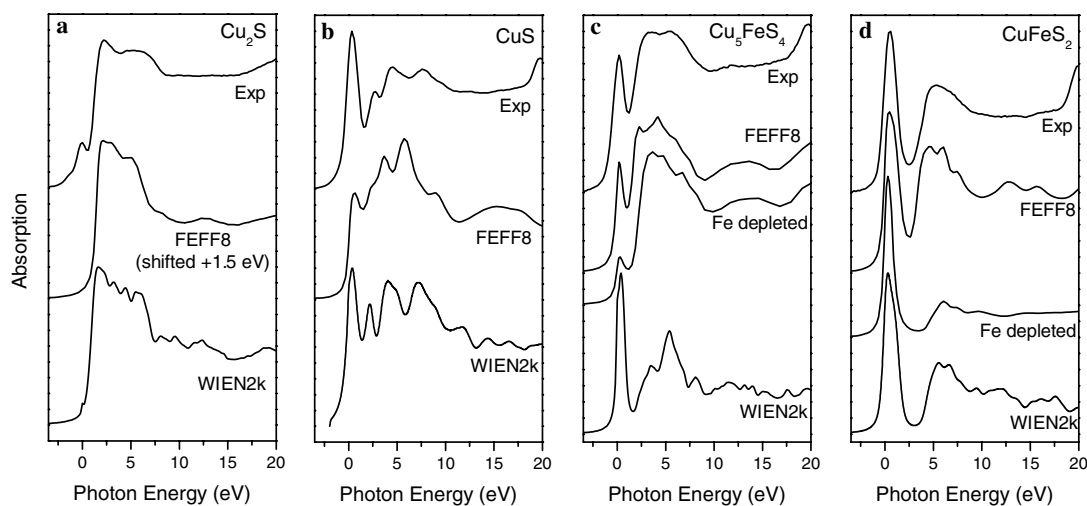


Fig. 9. Cu L<sub>3</sub>-edge NEXAFS spectra calculated using FEFF8 and WIEN2k for (a) chalcocite; (b) covellite; (c) bornite and Fe-depleted bornite; (d) chalcopyrite and Fe-depleted chalcopyrite.

tron spectra and O K-edge spectrum indicated very little surface oxidation, consistent with the similarity in the TEY and TFY Cu L-edge NEXAFS spectra. Indeed, the Cu 2p spectrum was similar for a freshly abraded surface, and for surfaces exposed to air for up to 1 h. The Cu  $L_3M_{4,5}M_{4,5}$  peak at a kinetic energy of 918.2 eV and Auger parameter of 1850.2 eV were both high but still within the range expected for Cu(I).

The FEFF8-simulated Cu  $L_3$ -edge spectrum for covellite, shown in Fig. 9b, is not in good agreement with the experimental spectrum. The most likely explanation is that the calculated Fermi level was too high, as it was for chalcocite. Although the claimed accuracy for calculating the Fermi level by means of FEFF8 is no better than 2 eV due to limitations such as the basis set and spherical potentials, the estimations appear to be accurate to better than 1 eV for all the sulfides investigated other than chalcocite and covellite. By contrast, WIEN2k calculations are able to simulate the Cu  $L_3$  spectrum for covellite reasonably well (Fig. 9b).

It should be noted that if CuS were to be considered as  $Cu_2S \cdot CuS_2$ , with the tetrahedrally coordinated Cu in  $Cu_2S$  assumed to be Cu(I) and the trigonally coordinated Cu in  $CuS_2$  assumed to be Cu(II), then it would be expected that the calculated contribution from Cu in the latter sites would have an initial absorption peak at a markedly lower energy and with markedly more intensity. This is not the case, therefore neither FEFF8 nor WIEN2k calculations provide any support for the proposition that some of the Cu in covellite is Cu(II). It is also important to note, for comparison with the spectra from bornite and chalcopyrite discussed below, that the leading absorption peak in the WIEN2k simulation arises predominantly from a relatively low density of Cu d-states but from a negligible density of Cu s-states. It is also evident from the calculated density of unfilled states that the peak near 935 eV (Figs. 6c and 7c) is due largely to transitions to minor Cu d- and S p-bands, and mostly from Cu in the four-coordinate sites. Thus, the interpretation by Todd et al. (2003b) of the Cu  $L_{2,3}$ -edge spectrum in terms of Cu(I) and Cu(II) is not supported.

Although FEFF8 calculations were unable to adequately simulate the Cu  $L_3$  spectrum for chalcocite or covellite, this situation does not apply for all Cu sulfides. In particular, the simulated spectrum for  $CuS_2$  agreed well with the experimentally determined spectrum reported by van der Laan et al. (1992). Therefore, there is no obvious reason for the inability of FEFF8 to simulate the Cu  $L_3$  spectra for  $Cu_2S$  and CuS; i.e., for the Fermi level calculated by FEFF8 to be  $\sim 2$  eV too high for those two sulfides.

### 3.3.4. Bornite

Although there were no significant differences in the peak positions in the TEY and TFY Cu  $L_{2,3}$  NEXAFS spectra for bornite exposed briefly to air (Figs. 6d and 7d), the leading peak at 932.7 eV was more intense in the TFY spectrum relative to the broad absorption above 934 eV. It has been inferred from XPS data that when

bornite is initially exposed to air, an iron oxide species is formed at the mineral/air interface to leave an iron-deficient sulfide layer between the oxide and the unaltered substrate (e.g., Buckley and Woods, 1983). The Fe 2p photoelectron spectrum (Fig. 3c) from the specimen examined by NEXAFS spectroscopy in this work is in agreement with this conclusion. Therefore it is possible that the TEY NEXAFS spectrum reflects a contribution from this Fe-deficient sulfide layer, a possibility that is supported by FEFF8 calculations (see below). The TEY Cu  $L_{2,3}$  spectrum in Fig. 6d was similar to the TEY spectrum for bornite obtained by Grioni et al. (1989) and van der Laan et al. (2002). It was quite different from the Cu  $L_{2,3}$  spectrum reported for synthetic  $Cu_5FeS_4$  by Mikhlin et al. (2005), almost certainly because that material would have been metal-rich. The metal-rich nature of the synthetic  $Cu_5FeS_4$  was deduced from a comparison of its Cu  $L_3$ -edge spectrum with the spectra published by van der Laan et al. (2002).

Neither the Cu 2p photoelectron spectrum (Fig. 8d) nor the Cu L-edge spectra provided any evidence for the presence of Cu(II) at the surface of the briefly air-exposed bornite. This is not in accord with the finding of Todd et al. (2000) that chalcocite and bornite both oxidise to form the same copper oxide product.

The FEFF8-simulated Cu  $L_3$ -edge spectrum for bornite, shown in Fig. 9c, is in reasonably good agreement with the experimental spectrum. There are 10 different Cu environments in bornite, but the spectra corresponding to the individual environments were not significantly different below 937 eV, and the overall (sum for all sites) spectrum is shown in Fig. 9c. Comparison of the *l*-DOS (Fig. 5a) with the simulated and experimental spectra reveals that the Fermi level is situated within a region of low but non-zero density of Cu d-states (as well as an even lower density of Cu s-states, a high density of Fe d-states and moderate density of S p-states). Thus, the *l*-DOS are consistent with the leading Cu  $L_3$  absorption peak arising predominantly from Cu d-states and consistent with the leading peak being at a relatively low energy. For bornite, the Cu  $L_3$ -edge spectrum simulated by FEFF8 is in better agreement with the experimental spectrum than that simulated using WIEN2k.

The Cu  $L_3$ -edge spectrum, also shown in Fig. 9c, for an Fe depleted, but otherwise unaltered bornite lattice calculated using FEFF8 indicated that a less intense leading absorption peak would be expected from such an altered layer, unlike the situation for an Fe-depleted chalcopyrite lattice (Fig. 9d). The trend for vacancies in only one of the two Fe sites in bornite was the same. This is consistent with the difference in the TEY and TFY Cu  $L_3$  absorption spectra. However, in apparent disagreement with this finding, the TEY Cu  $L_3$  spectra from synthetic Fe-deficient and Cu-rich bornite specimens reported by van der Laan et al. (2002) displayed a leading absorption peak that was more intense than that for a near-stoichiometric bornite sample. Also, the leading absorption peak in the Cu  $L_3$ -edge spectrum for leached synthetic  $Cu_5FeS_4$  observed by Mikhlin et al. (2005) was more intense than that for the untreated

natural bornite investigated here. It is possible that in the former case, the effect of excess Cu was greater than that of Fe deficiency, and in the latter case, some restructuring of the Fe-deficient sulfide lattice had taken place. It is also possible that the effect of metal depletion in one or both Fe lattice sites was too extreme for deducing the trend for Fe deficiency, notwithstanding the agreement with the difference between the TEY and TFY spectra.

### 3.3.5. Chalcopyrite

The TEY and TFY Cu  $L_{2,3}$ -edge NEXAFS spectra for freshly abraded chalcopyrite exposed to air for no more than a few minutes (Figs. 6e and 7e) were essentially the same. The spectra were qualitatively similar to those determined previously, however the leading absorption peak was at 932.6 eV compared with values ranging from 932.4 to 932.7 eV (Grioni et al., 1989; van der Laan et al., 1992; Patrick et al., 1997; Todd et al., 2003b; Mikhlin et al., 2004). Grioni et al. (1989) and Schmidt et al. (2001) observed the leading absorption peak at the same photon energy as for bornite, whereas van der Laan et al. (1992) observed the position of this peak for chalcopyrite to be 0.6 eV higher than for bornite. Therefore, there is no evidence that the absorption energy for chalcopyrite is more than 0.3 eV lower than it is for bornite. Moreover, the leading absorption peak for chalcopyrite is no broader than the corresponding peak for bornite. Since there are no grounds for suggesting that the copper in bornite is present as Cu(II), it follows that there is no justification for assigning the copper in chalcopyrite to Cu(II) on the basis of its Cu L-edge absorption energy.

The Cu 2p photoelectron spectrum from the same chalcopyrite specimen (Fig. 8e) confirmed that Cu(II)-oxygen species were not present at the surface. It should be noted that the Cu  $2p_{3/2}$  binding energy of 932.1 eV being  $\sim 0.3$  eV lower than the value for bornite provides no support for the proposition that the Cu in  $\text{CuFeS}_2$  is more like Cu(II) relative to the Cu in  $\text{Cu}_5\text{FeS}_4$ . The TEY and TFY Cu  $L_{2,3}$ -edge spectra for chalcopyrite exposed to air for several hours were also essentially the same, confirming that Cu oxide species had not been formed within the surface layer during the additional exposure period.

The FEFF8-simulated Cu  $L_3$ -edge spectrum for chalcopyrite, shown in Fig. 9d, is in very good agreement with the experimental spectrum. The calculated Fermi level lies  $\sim 1.6$  eV below the end of a region of low (but non-zero) density of Cu d- and s-states, as well as within a high density of Fe d-states and moderate density of S p-states. Therefore, it is not surprising that the leading Cu  $L_3$  absorption peak for chalcopyrite is at almost the same low energy as it is for bornite. It can be deduced from the calculated density of states shown in Fig. 5b that the broader Cu  $L_3$  peak situated  $\sim 5$  eV above the leading absorption peak would arise from transitions to Cu s-states and, to a lesser extent, Cu d-states. Most of the previous electronic structure calculations for chalcopyrite, including those using FEFF8 with the Hedin–Lundqvist exchange

potential (Lavrentyev et al., 2004), are in broad agreement with the FEFF8 calculations carried out in the present study (Hamajima et al., 1981; Tossell et al., 1982; Petiau et al., 1988; Kurmaev et al., 1998; Edelbro et al., 2003).

The WIEN2k-simulated Cu  $L_3$ -edge spectrum (Fig. 9d) also closely resembles the experimental spectrum. The densities of unfilled states (Fig. 5b) were similar to those calculated by FEFF8 except for the Cu d-DOS which was more than five times greater, consistent with the relative intensity of the leading Cu  $L_3$ -edge peak being higher than that calculated by FEFF8, and even higher than that for the experimental spectrum. For this investigation, it is crucial to note that a comparison of the WIEN2k-calculated Cu d-DOS for  $\text{Cu}_2\text{S}$  and  $\text{CuFeS}_2$  reveals that a similarly low Cu d-DOS is able to explain the Cu L-edge leading peak for both  $\text{Cu}_2\text{S}$  and for  $\text{CuFeS}_2$ , i.e., without the need to invoke the admixture of Fe d-states for the latter. Thus, the considerable difference in the leading Cu  $L_3$ -edge absorption peaks observed for these two sulfides does not arise from any fundamental difference in the final state of the electronic transition or from a difference in Cu formal oxidation state.

Mikhlin et al. (2005) interpreted their Cu L-edge spectra for chalcopyrite (and leached bornite) as indicating a formal Cu valence between +1 and +2, although they noted that the Cu(II) quantity remained as low as a few percent. This interpretation is discussed further in Section 3.6.

### 3.4. S K-edge NEXAFS spectra

Even though S electronic environments were not the main focus of this investigation, it was pertinent to determine the S K-edge NEXAFS spectra in order to assess the ability of FEFF8 to simulate those spectra, and to potentially obtain complementary information on the unfilled density of states of the Cu and Cu–Fe sulfides. The TFY S K-edge spectra from pyrite, pyrrhotite, chalcocite, covellite, bornite and chalcopyrite are shown in Fig. 10a–f, respectively. The corresponding simulated spectra calculated using FEFF8 are also shown in Fig. 10. Apart from that for chalcocite, the experimental spectra are generally in good agreement with the corresponding spectra reported previously, such as those by Sugiura (1981), Petiau et al. (1988), Li et al. (1994, 1995), Mosselmans et al. (1995), Patrick et al. (1997), Lavrentyev et al. (2004) and von Oertzen et al. (2005).

It can be seen from Fig. 10 that FEFF8 calculations were able to simulate the experimental S K-edge spectra reasonably well, including the energy of each leading absorption peak, with the possible exception of covellite. Most importantly for this investigation, the FEFF8 S K-edge simulations for bornite and chalcopyrite were acceptable, thereby providing further evidence that the calculated densities of states for these two sulfides were applicable. The simulated spectrum for  $\text{FeS}_2$  was in good agreement with that reported by Hallmeier et al. (2002), and the simulated spectra for  $\text{FeS}_2$ , CuS and  $\text{CuFeS}_2$  are similar to

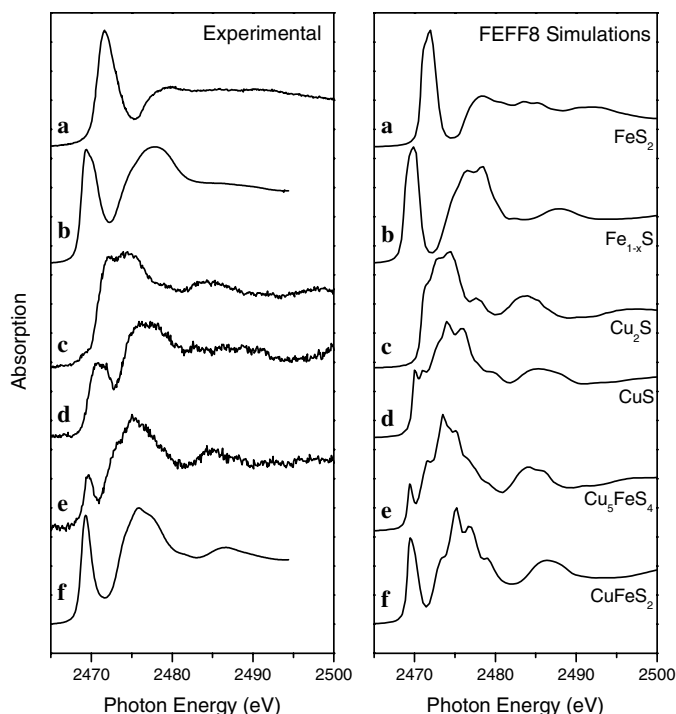


Fig. 10. TFY and FEFF8-simulated S K-edge NEXAFS spectra for (a) pyrite; (b) pyrrhotite; (c) chalcocite; (d) covellite; (e) bornite; (f) chalcopyrite.

those calculated by Lavrentyev et al. (2004) using FEFF8 with the Hedin–Lundqvist exchange potential.

### 3.5. O K-edge NEXAFS spectra

In obtaining reliable O K-edge spectra for oxygen-containing species present only at the surface of a specimen, it is important to ensure that artefacts are not introduced from any oxygen present in the beam-line such as on the mesh used to monitor  $I_0$ . To ensure that this was not the case in the present work, the O K-edge spectrum from a freshly cleaved surface of molybdenite was obtained under the same experimental conditions. When normalised by  $I_0$  monitored by means of the gold-coated mesh, the O K-edge spectrum from the molybdenite basal planes was featureless as expected.

Energy calibration in the O K-edge range is less well defined than for many other edges, but leading absorption peak energies for  $\text{TiO}_2$  and  $\text{CuO}$  are often used. The 530.1 eV value reported by Karppinen et al. (2001) for  $\text{CuO}$  appears to be reliable and is in close agreement with the 530.2 eV obtained by Todd et al. (2003b) for tenorite. Accordingly, the leading absorption peak energy of 530.2 eV for  $\text{FeOOH}$  and  $\text{Fe}_2\text{O}_3$  reported by Todd et al. (2003b), rather than the value of 529.8 eV quoted earlier by Todd et al. (2003a), has been adopted here. A value close to 530 eV for  $\text{FeOOH}$  is consistent with the O K-edge spectrum shown by Doyle et al. (2004). It should be noted, however, that different values for  $\text{CuO}$  and  $\text{Fe}_2\text{O}_3$  have been reported, including 530.5 eV for  $\text{CuO}$  by Schedel-

Niedrig et al. (2000) and also for  $\text{Fe}_2\text{O}_3$  by Chen et al. (1996). Nevertheless, these small differences have no overall bearing on the conclusions drawn from the O K-edge spectra obtained in the present investigation.

#### 3.5.1. Pyrrhotite

As noted in Section 3.2.2, pyrrhotite was investigated not only as another reference Fe(II) sulfide, but also as a reference for surface rather than bulk iron oxide species. The TEY O K-edge spectrum from a pyrrhotite surface exposed to air for no more than a few minutes is shown in Fig. 11a. As expected from XPS data, and from the likely amorphous nature of the surface iron oxide species, this spectrum is similar to a superposition of O K-edge spectra from hematite and goethite, such as those reported by Todd et al. (2003a,b) and Doyle et al. (2004), but without clear resolution of any fine structure near 530 and 531.5 eV in the leading absorption peak at  $\sim 530.7$  eV. The spectrum in Fig. 11a is quite similar to that obtained by Mikhlin and Tomashevich (2005) for monoclinic pyrrhotite abraded in air.

The formation of Fe(II) oxide is not expected at the surface of air-exposed pyrrhotite, however its presence on the basis of the O K-edge spectrum alone could probably not be excluded. There are subtle differences in the O K-edge spectra from bulk  $\text{FeO}$  and  $\text{Fe}_2\text{O}_3$  (Chen et al., 1996), for

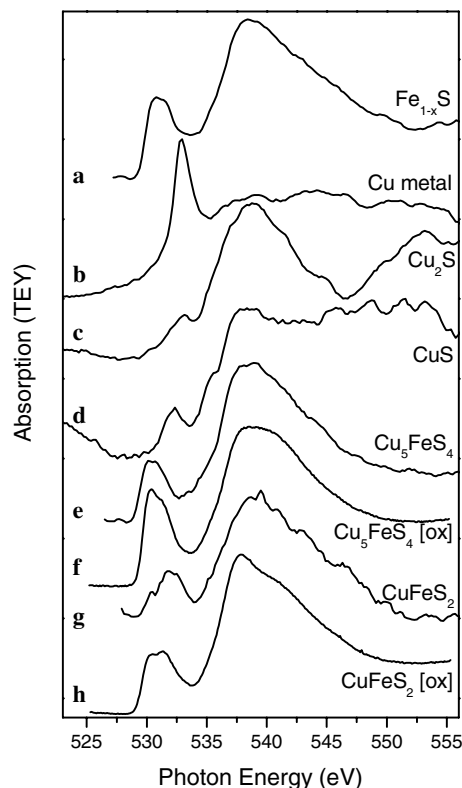


Fig. 11. TEY O K-edge NEXAFS spectrum, for surface exposed briefly to air unless otherwise stated, of (a) pyrrhotite; (b) copper metal; (c) chalcocite; (d) covellite; (e) bornite; (f) bornite exposed for 24 h; (g) chalcopyrite; (h) chalcopyrite exposed for 24 h.

example, however it is unlikely that Fe(II) and Fe(III) oxide could be differentiated in a surface oxidation layer, especially as the oxide species would probably be amorphous.

### 3.5.2. Copper metal, chalcocite and covellite

The O K-edge spectrum from the air-exposed Cu metal surface described in Section 3.3.1 displayed only one sharp absorption peak at  $\sim 532.9$  eV (Fig. 11b) arising from the predominant  $\text{Cu}_2\text{O}$  identified in the Cu L-edge spectrum. The position of this peak is in reasonable agreement with some published values for bulk  $\text{Cu}_2\text{O}$  (e.g., Gurevich et al., 1999; Todd and Sherman, 2003), but not the PEY value of 533.8 eV reported by Schedel-Niedrig et al. (2000). As expected, given the low surface concentration of Cu(II) species revealed by the Cu 2p photoelectron and Cu L-edge spectra, a second O K-edge absorption peak nearer to 530 eV from CuO was not observed.

The O K-edge spectrum from chalcocite exposed briefly to air (Fig. 11c) displayed a weak but sharp absorption peak near 533 eV preceding a relatively intense broader absorption peak at  $\sim 538$  eV. The absence of a discernible peak near 530 eV indicated that CuO was not the principal oxide species present at the mineral surface. Furthermore, the relatively high intensity of the broad peak near 538 eV was not consistent with the O K-edge spectrum for  $\text{Cu}_2\text{O}$  reported by Gurevich et al. (1999) or Todd et al. (2003b). Rather, it resembled the spectrum for basic copper carbonate (azurite) reported by Todd and Sherman (2003). It was also similar to the spectrum for copper sulfate (Todd and Sherman, 2003; Todd et al., 2003b), but sulfate at the surface of chalcocite exposed to air for up to 24 h had not been detected by XPS (Buckley et al., 2003). Neither of these O K-edge spectra displayed a peak near 530 eV. Therefore, it appears that a clearly discernible O K-edge peak near 530 eV is not a necessary indicator of Cu(II) bonded to oxygen.

The O K-edge absorption peak from covellite exposed briefly to air (Fig. 11d) was of low intensity and at an energy  $\sim 0.7$  eV lower than that for chalcocite. There was no evidence for an additional absorption peak near 530 eV that might have arisen from any CuO present, an observation consistent with the Cu 2p photoelectron and Cu L-edge absorption spectra. An additional peak near 530 eV was not observed even for a specimen that had been exposed to air for several hours, but the broad, relatively intense absorption peak at  $\sim 539$  eV suggested that another Cu(II)–oxygen species such as carbonate may have been formed.

### 3.5.3. Bornite

The O K-edge spectrum for bornite exposed briefly to air (Fig. 11e) was similar to that for briefly exposed pyrrhotite, the only minor difference being a lower intensity of the leading absorption peak (near 530.4 eV) relative to the main absorption peak. The presence of some Cu–oxygen species such as CuO in addition to the oxidised Fe could

not be excluded on the basis of the O K-edge spectra alone, however, the presence of a significant concentration of Cu–oxygen species in the surface layer can be excluded on the basis of the similarity of the TEY and TFY Cu L-edge spectra, apart from a more intense leading peak at  $\sim 933$  eV in the TFY spectrum. That additional intensity was consistent with a contribution from a sub-surface iron-depleted copper sulfide phase, but inconsistent with less influence from any surface copper oxide species that might have been present. Thus, the O K-edge spectrum for briefly air-exposed bornite is entirely consistent with the Fe and Cu L-edge spectra and the presence of surface Fe oxide species. The leading absorption peak in the O K-edge spectrum for bornite exposed to air for 24 h (Fig. 11f) was also similar to the spectrum from pyrrhotite (Fig. 11a).

Mikhlin et al. (2005) concluded that, by comparison with previously published O K-edge spectra from copper and iron oxides, as well as from oxidised chalcopyrite and pyrite, the O K-edge spectrum from air-exposed bornite indicated the presence of Cu(I) oxide and Cu(II) oxide rather than Fe oxides. In particular, they attributed peaks at 530.5, 535.9 and 540 eV to CuO, and peaks at 533.8, 535.7 and 539.6 eV to  $\text{Cu}_2\text{O}$ , on the basis of the data reported by Schedel-Niedrig et al. (2000). However, the  $\text{Cu}_5\text{FeS}_4$  studied by Mikhlin et al. (2005) was synthetic material that the Cu L-edge spectrum revealed (van der Laan et al., 2002) was non-stoichiometric and most probably Cu-rich. Hence copper oxide formation at such a surface might not be typical of natural, near-stoichiometric bornite. Todd et al. (2000) also claimed that the Cu L-edge and O K-edge spectra for  $\text{Cu}_2\text{S}$  and  $\text{Cu}_5\text{FeS}_4$  revealed that these minerals oxidised to the same compound that they tentatively assigned to CuO, and that the absence of surface iron was confirmed by the Fe L-edge spectrum from bornite. Those claims have not been supported by the data presented above and in Section 3.2.3.

### 3.5.4. Chalcopyrite

The O K-edge spectrum from chalcopyrite exposed to air for no more than a few minutes (Fig. 11g) was quite similar to O K-edge spectra from pyrrhotite and bornite exposed briefly to air (Figs. 11a and e). The O K-edge spectra from chalcopyrite surfaces exposed to air for extended periods (e.g., Fig. 11h) were also similar to that for oxidised pyrrhotite. In fact none of the O K-edge spectra was more consistent with a Cu oxide than with an Fe oxide species, whereas the metal 2p photoelectron spectra and metal L-edge spectra were all more consistent with the presence of Fe rather than Cu initial oxidation products at an air-exposed chalcopyrite surface. In particular, the TEY and TFY Cu L-edge spectra were essentially the same for chalcopyrite exposed to air for less than a day, confirming the absence of Cu oxide species in the surface layer.

Although the O K-edge spectra obtained by Todd et al. (2003b) from chalcopyrite exposed to air for at least 7 days resembled the O K-edge spectrum for goethite, the chalcop-

pyrite spectra were complex, and were interpreted as indicating the presence of both copper and iron oxide and sulfate species. However, even if that interpretation were correct, it does not necessarily mean that copper oxide species are formed on chalcopyrite exposed to air for significantly shorter periods. Similarly, England et al. (1999) obtained Cu K-edge glancing-angle X-ray absorption spectra that revealed the formation of Cu oxide species at the surface of chalcopyrite, but only after the mineral had been electrochemically oxidised.

### 3.6. Formal oxidation states of Cu and Fe in chalcopyrite and bornite

The formal oxidation states Cu(I) and Cu(II) correspond to predominantly  $3d^{10}$  and  $3d^9$  ground state configurations, while Fe(II) and Fe(III) correspond to  $3d^6$  and  $3d^5$  configurations, respectively. Provided the ab initio calculations are able to adequately simulate the experimental NEXAFS spectra, the calculated DOS, particularly the d-DOS, should provide a reliable indication of any significant differences in formal oxidation state between those sulfides having an unambiguous formal oxidation state and those that are subject to doubt. In principle, it is the self-consistent field estimate of the charge transfer and orbital occupancy in the particular lattice in the presence of the core hole that should be relevant, although it has been established that for the  $L_{2,3}$ -edges of Co, Ni and Cu, FEFF8 calculations without the core hole provide better agreement with experimental data (Nesvizhskii and Rehr, 1999). In practice, however, the calculated data for Cu(I) and Cu(II) oxides (Table 3) suggest that comparison of orbital occupancies is not straightforward. The spectator Cu 3d occupancies for Cu,  $Cu_2O$  and CuO were found to be essentially the same at  $\sim 9.7$ . For absorbing Cu atoms, the 3d occupancies for  $Cu_2O$  and CuO were also very similar at  $10.30 \pm 0.01$  or  $10.22 \pm 0.01$  depending on the exchange potential used.

The Cu 2p photoelectron spectrum, Cu LMM Auger spectrum and Cu Auger parameter ( $2p_{3/2}$  binding energy +  $L_3M_{4,5}M_{4,5}$  kinetic energy) for neither chalcopyrite nor bornite are indicative of Cu(II). The values of the Auger parameter obtained for the two copper-iron sulfides were 1849.8 and 1849.7 eV, respectively, whereas those for chalcocite and covellite were 1849.7 and 1850.3 eV. There is no known report of an Auger parameter less than 1850.5 eV for a copper compound with an unambiguous Cu(II) formal oxidation state.

The calculated unfilled states immediately above the Fermi level should correlate with the orbital occupancies. The leading Cu  $L_3$ -edge peak in Cu(I) sulfides such as bornite has been attributed by van der Laan et al. (2002) to transitions between the Cu  $2p^63d^{10}4s^1\bar{S}$ -like ground state and Cu  $2p^53d^{10}4s^2\bar{S}$ -like final state, S-hole configurations. Mikhlin et al. (2005), on the other hand, assigned such a leading peak to transitions between Cu  $2p^63d^9$ - and Cu  $2p^53d^{10}$ -like states associated with the “few percent of

Cu(II)” inherent in the sulfide that contribute disproportionately to the Cu L-edge absorption spectrum because of the relatively high transition probability, but are not evident in the Cu 2p photoelectron spectrum. The calculations reported here for chalcopyrite and bornite indicate a very low density of Cu s-states immediately above the Fermi level, as well as a medium level of S p-states and a high level of Fe d-states. For chalcopyrite, the FEFF8 calculations predict a density of Cu d-states significantly lower than that for the S p-states, whereas the WIEN2k calculations estimate the density of Cu d-states to be somewhat higher and at least as great as for the S p-states. Since the form of the experimental Cu  $L_3$ -edge spectrum lies between those simulated by FEFF8 and WIEN2k, it is reasonable to deduce that the actual density of states immediately above the Fermi level lies between those predicted by FEFF8 and WIEN2k. On that basis, the actual density of Cu d-states would be greater than the density of Cu s-states, and comparable with the density of S p-states, but an order of magnitude lower than the density of Fe d-states. Taking into account the fact that the Cu  $L_3$ -edge spectra for chalcocite and covellite can be simulated by a similarly low density of Cu d-states, then the leading absorption peak in the Cu  $L_3$ -edge spectrum for chalcopyrite can also be rationalised in terms of the Cu d occupancy, and there is no need to invoke the involvement of Fe d-states. This conclusion is in broad agreement with the explanation proposed by Mikhlin et al. (2005), however to equate a small density of Cu d-states above the Fermi level as the presence of “a few percent of Cu(II)” is not regarded as a meaningful concept for a structure like that of chalcopyrite or bornite, whereas it might possibly be justified for a structure like  $Cu_{1.96}S$ . If bornite were considered to be  $Cu_4^I Cu^{II} Fe^{III} S_4$ , rather than  $Cu_5^I Fe^{III} S_4$ , to allow for some inherent Cu(II), there should be some other evidence for the non-equivalence of 20% of Cu atoms. In particular, as already noted, the presence of 20% of copper being in a formal oxidation state of Cu(II) is not consistent with the Cu 2p photoelectron spectrum, or indeed the Cu L-edge NEXAFS spectrum.

Given that there is no compelling argument for 20% of the Cu in bornite to be Cu(II), nor for the Cu in chalcopyrite to be regarded as Cu(II), then there is no justification on this basis for regarding the Fe in these two sulfides as having a formal oxidation state of Fe(II). There is also no justification on the basis of the energy of the leading absorption peak of the Fe  $L_3$ -edge spectrum, as illustrated by the  $L_3$ -edge spectra for pyrite, goethite and hematite. Nevertheless, as concluded by Fujisawa et al. (1994), there is ample evidence to suggest that although the iron in chalcopyrite is formally Fe(III), there is significant S  $3p \rightarrow Fe$  3d charge transfer. This would lead to lower and higher electron densities on the S and Fe atoms, respectively, than might have been expected. This situation is consistent with the FEFF8-calculated charge transferred, but the agreement may be fortuitous. Similarly, Hall and Stewart (1973) considered that there was stereochemical evidence for chalcopyrite having strong covalent bonds but with

an effective ionic state between  $\text{Cu}^+\text{Fe}^{3+}\text{S}_2$  and  $\text{Cu}^{2+}\text{Fe}^{2+}\text{S}_2$  and closer to the latter than the former.

#### 4. Conclusions

Ab initio calculations for chalcopyrite and bornite indicate that the densities of Cu d-states immediately above the Fermi level are low but sufficient to account for the Cu  $L_{2,3}$ -edge absorption spectra. Nevertheless, no convincing evidence was obtained for chalcopyrite to be represented as  $\text{Cu}^{\text{II}}\text{Fe}^{\text{II}}\text{S}_2$ , or for some of the Cu in either bornite or covellite to be regarded as Cu(II). The X-ray absorption spectra were quite consistent with the initial oxidation products on chalcopyrite and bornite surfaces being iron oxide and hydroxyoxide, and inconsistent with the concomitant formation of copper oxide species. FEFF8 calculations, mostly with an unscreened core hole, were able to simulate the experimental NEXAFS spectra quite well in almost all cases. For CuS and  $\text{Cu}_2\text{S}$ , it was found that FEFF8 did not provide a good simulation of the Cu  $L_3$ -edge spectra, but WIEN2k simulations were in close agreement with the experimental data. Neither the FEFF8-calculated d occupancy nor total charge on the Fe atoms was useful for differentiating formal oxidation states of Fe in the sulfide minerals. For copper, the calculated total charge on the Cu atoms appeared to be an indicator of formal oxidation state, but the differences were too small to be reliable.

#### Acknowledgments

This work was supported by the Australian Synchrotron Research Program, which is funded by the Commonwealth of Australia under the Major National Research Facilities Program. Use of the Advanced Photon Source was supported by the US Department of Energy, Office of Science, Office of Basic Energy Sciences, under Contract No. W-31-109-ENG-38. The assistance of XOR staff J.W. Freeland, D.J. Keavney, P. Ryan and D. Haskell, and NSRRC BL24A personnel Y.-w. Yang, L.-J. Fan and L.-J. Lai, is gratefully acknowledged. The authors are grateful for computational help from H.S. Chan, and for advice on the application of FEFF8 provided by J. Rehr and B. Gilbert, with particular thanks to A.L. Ankudinov for his suggestion to use an excited initial configuration for Fe for charge transfer calculations. The authors are also indebted to P. Blaha for his considerable help in enabling WIEN2k calculations to be carried out on a PC at the UNSW and to V. Keast for advice on using WIEN2k.

Associate editor: David J. Vaughan

#### References

Ankudinov, A.L., Bouldin, C.E., Rehr, J.J., Sims, J., Hung, H., 2002. Parallel calculation of electron multiple scattering using Lanczos algorithms. *Phys. Rev. B* **65**, 104107-1–104107-11.

- Bayliss, P., 1977. Crystal structure refinement of a weakly anisotropic pyrite. *Am. Miner.* **62**, 1168–1172.
- Blaha, P., Schwarz, K., Sorantin, P., Trickey, S.B., 1990. Full-potential, linearized augmented plane wave programs for crystalline systems. *Comput. Phys. Commun.* **59**, 399–415.
- Boursiquot, S., Mullet, M., Abdelmoula, M., Génin, J.-M., Ehrhardt, J.-J., 2001. The dry oxidation of tetragonal  $\text{FeS}_{1-x}$  mackinawite. *Phys. Chem. Miner.* **28**, 600–611.
- Brion, D., 1980. Etude par spectroscopie de photoelectrons de la dégradation superficielle de  $\text{FeS}_2$ ,  $\text{CuFeS}_2$ ,  $\text{ZnS}$  et  $\text{PbS}$  à l'air et dans l'eau. *Appl. Surf. Sci.* **5**, 133–152.
- Buckley, A.N., Woods, R., 1983. An X-ray photoelectron spectroscopic investigation of the tarnishing of bornite. *Aust. J. Chem.* **36**, 1793–1804.
- Buckley, A.N., Woods, R., 1984. An X-ray photoelectron spectroscopic study of the oxidation of chalcopyrite. *Aust. J. Chem.* **37**, 2403–2413.
- Buckley, A.N., Woods, R., 1985. X-ray photoelectron spectroscopy of oxidized pyrrhotite surfaces. I. Exposure to air. *Appl. Surf. Sci.* **22/23**, 280–287.
- Buckley, A.N., Woods, R., 1987. The surface oxidation of pyrite. *Appl. Surf. Sci.* **27**, 437–452.
- Buckley, A.N., Goh, S.W., Lamb, R.N., Woods, R., 2003. Interaction of thiol collectors with pre-oxidised sulfide minerals. *Int. J. Miner. Process.* **72**, 163–174.
- Charnock, J.M., Henderson, C.M.B., Mosselmans, J.F.W., Patrick, R.A.D., 1996. 3d transition metal L-edge X-ray absorption studies of the dichalcogenides of Fe, Co and Ni. *Phys. Chem. Miner.* **23**, 403–408.
- Chen, J.G., Frühberger, B., Colaianni, M.L., 1996. Near-edge X-ray absorption fine structure characterization of compositions and reactivities of transition metal oxides. *J. Vac. Sci. Technol.* **14**, 1668–1673.
- Doyle, C.S., Kendelwicz, T., Bostick, B.C., Brown Jr, G.E., 2004. Soft X-ray spectroscopic studies of the reaction of fractured pyrite surfaces with Cr(VI)-containing aqueous solutions. *Geochim. Cosmochim. Acta* **68**, 4287–4299.
- Edelbro, R., Sandström, Å, Paul, J., 2003. Full potential calculations on the electron band structures of sphalerite, pyrite and chalcopyrite. *Appl. Surf. Sci.* **206**, 300–313.
- England, K.E.R., Charnock, J.M., Patrick, R.A.D., Vaughan, D.J., 1999. Surface oxidation studies of chalcopyrite and pyrite by glancing-angle X-ray absorption spectroscopy (REFLEXAFS). *Min. Mag.* **63**, 559–566.
- Evans Jr., H.T., 1971. Crystal structure of low chalcocite. *Nature* **232**, 69–70.
- Evans Jr., H.T., 1979. Djurleite ( $\text{Cu}_{1.94}\text{S}$ ) and low chalcocite ( $\text{Cu}_2\text{S}$ ): new crystal structure studies. *Science* **203**, 356–358.
- Evans Jr., H.T., Konnert, J.A., 1976. Crystal structure refinement of covellite. *Am. Miner.* **61**, 996–1000.
- Eyert, V., Höck, K.-H., Fiechter, S., Tributsch, H., 1998. Electronic structure of  $\text{FeS}_2$ : the crucial role of electron–lattice interaction. *Phys. Rev. B* **57**, 6350–6359.
- Folmer, J.C.W., Jellinek, F., 1980. The valence of copper in sulphides and selenides: an X-ray photoelectron spectroscopy study. *J. Less-Common Met.* **76**, 153–162.
- Folmer, J.C.W., Jellinek, F., Calis, G.H.M., 1988. The electronic structure of pyrites, particularly  $\text{CuS}_2$  and  $\text{Fe}_{1-x}\text{Cu}_x\text{Se}_2$ : an XPS and Mössbauer study. *J. Solid State Chem.* **72**, 137–144.
- Frazer, B.H., Gilbert, B., Sonderegger, B.R., De Stasio, G., 2003. The probing depth of total electron yield in the sub-keV range: TEY-XAS and X-PEEM. *Surf. Sci.* **537**, 161–167.
- Fujisawa, M., Suga, S., Mizokawa, T., Fujimori, A., Sato, K., 1994. Electronic structure of  $\text{CuFeS}_2$  and  $\text{CuAl}_{0.9}\text{Fe}_{0.1}\text{S}_2$  studied by electron and optical spectroscopies. *Phys. Rev. B* **49**, 7155–7164.
- Gebhardt, J.E., McCarron, J.J., Richardson, P.E., Buckley, A.N., 1986. The effect of cathodic treatment on the anodic polarization of copper sulfides. *Hydrometallurgy* **17**, 27–38.
- Goble, R.J., 1985. The relationship between crystal structure, bonding and cell dimensions in the copper sulfides. *Can. Miner.* **23**, 61–76.

- Grioni, M., Goedkoop, J.B., Schoorl, R., de Groot, F.M.F., Fuggle, J.C., Schäfers, F., Koch, E.E., Rossi, G., Esteve, J.-M., Karnatak, R.C., 1989. Studies of copper valence states with Cu  $L_3$  X-ray-absorption spectroscopy. *Phys. Rev. B* **39**, 1541–1545.
- Gurevich, A.B., Bent, B.E., Teplakov, A.V., Chen, J.G., 1999. A NEXAFS investigation of the formation and decomposition of CuO and Cu<sub>2</sub>O thin films on Cu(100). *Surf. Sci.* **442**, L971–L976.
- Hall, S.R., Stewart, J.M., 1973. The crystal structure refinement of chalcopyrite, CuFeS<sub>2</sub>. *Acta Cryst. B* **29**, 579–585.
- Hallmeier, K.H., Uhlig, I., Szargan, R., 2002. Sulphur  $L_{2,3}$  and  $L_1$  XANES investigations of pyrite and marcasite. *J. Electron Spectrosc.* **122**, 91–96.
- Hamajima, T., Kambara, T., Gondaira, K.I., Oguchi, T., 1981. Self-consistent electronic structures of magnetic semiconductors by a discrete variational  $X\alpha$  calculation. *Phys. Rev. B* **24**, 3349–3353.
- Jellinek, F., 1972. Sulphides, selenides and tellurides of the transition Elements. In: D.W.A. Sharp (Ed.), Medical and Technical Publishing International Review of Science, Inorganic Chemistry Series One, vol. 5. Butterworths, Oxford, University Park Press, Baltimore, pp. 339–396.
- Karppinen, M., Kotiranta, M., Yamauchi, H., Nachimuthu, P., Liu, R.S., Chen, J.M., 2001. O K-edge and Cu  $L_{2,3}$ -edge XANES study on the concentration and distribution of holes in the (Pb<sub>2/3</sub>Cu<sub>1/3</sub>)<sub>3</sub>Sr<sub>2</sub>(Y,Ca)-Cu<sub>2</sub>O<sub>8+z</sub> superconductive phase. *Phys. Rev. B* **63**, 184507-1–184507-6.
- King Jr., H.E., Prewitt, C.T., 1979. Structure and symmetry of CuS<sub>2</sub> (pyrite structure). *Am. Miner.* **64**, 1265–1271.
- Koto, K., Morimoto, N., 1975. Superstructure investigation of bornite, Cu<sub>5</sub>FeS<sub>4</sub>, by the modified partial Patterson function. *Acta Cryst. B* **31**, 2268–2273.
- Kurmaev, E.Z., van Ek, J., Ederer, D.L., Zhou, L., Callcott, T.A., Perera, R.C.C., Cherkashenko, V.M., Shamin, S.N., Trofimova, V.A., Bartkowski, S., Neumann, M., Fujimori, A., Moloshag, V.P., 1998. Experimental and theoretical investigation of the electronic structure of transition metal sulphides: CuS, FeS<sub>2</sub> and FeCuS<sub>2</sub>. *J. Phys.: Condens. Matter* **10**, 1687–1697.
- Lavrentyev, A.A., Gabrelian, B.V., Nikiforov, I.Ya., Rehr, J.J., Ankudinov, A.L., 2004. The electron energy structure of some sulfides of iron and copper. *J. Electron Spectrosc.* **137–140**, 495–498.
- Lawniczac-Jablonska, K., Perera, R.C.C., Underwood, J.H., Gullikson, E.M., Iwanowski, R.J., 1997. Hybridization of the 3d states of transition metals with the states of the ZnS matrix. *Phys. Rev. B* **55**, 10376–10381.
- Li, D., Bancroft, G.M., Kasrai, M., Fleet, M.E., Feng, X., Tan, K., 1995. S K- and L-edge X-ray absorption spectroscopy of metal sulfides and sulfates: applications in mineralogy and geochemistry. *Can. Miner.* **33**, 949–960.
- Li, D., Bancroft, G.M., Kasrai, M., Fleet, M.E., Feng, X.H., Yang, B.X., Tan, K.H., 1994. S K- and L-edge XANES and electronic structure of some copper sulfide minerals. *Phys. Chem. Miner.* **21**, 317–324.
- Mikhlin, Y., Tomashevich, Y., 2005. Pristine and reacted surfaces of pyrrhotite and arsenopyrite as studied by X-ray absorption near-edge structure spectroscopy. *Phys. Chem. Miner.* **32**, 19–27.
- Mikhlin, Y.L., Tomashevich, Y.V., Asanov, I.P., Okotrub, A.V., Varnek, V.A., Vyalikh, D.V., 2004. Spectroscopic and electrochemical characterization of the surface layers of chalcopyrite (CuFeS<sub>2</sub>) reacted in acidic solutions. *Appl. Surf. Sci.* **225**, 395–409.
- Mikhlin, Y., Tomashevich, Y., Tauson, V., Vyalikh, D., Molodtsov, S., Szargan, R., 2005. A comparative X-ray absorption near-edge structure study of bornite, Cu<sub>5</sub>FeS<sub>4</sub>, and chalcopyrite, CuFeS<sub>2</sub>. *J. Electron Spectrosc.* **142**, 83–88.
- Mosselmans, J.F.W., Patrick, R.A.D., van der Laan, G., Charnock, J.M., Vaughan, D.J., 1995. X-ray absorption near-edge spectra of transition metal disulfides FeS<sub>2</sub> (pyrite and marcasite), CoS<sub>2</sub>, NiS<sub>2</sub> and CuS<sub>2</sub>, and their isomorphs FeAsS and CoAsS. *Phys. Chem. Miner.* **22**, 311–317.
- Nakai, I., Sugitani, Y., Nagashima, K., Niwa, Y., 1978. X-ray photoelectron spectroscopic study of copper minerals. *J. Inorg. Nucl. Chem.* **40**, 789–791.
- Nesvizhskii, A.I., Rehr, J.J., 1999. L-edge XANES of 3d-transition metals. *J. Synchrotron Rad.* **6**, 315–316.
- Patrick, R.A.D., van der Laan, G., Vaughan, D.J., Henderson, C.M.B., 1993. Oxidation state and electronic configuration determination of copper in tetrahedrite group minerals by L-edge X-ray absorption spectroscopy. *Phys. Chem. Miner.* **20**, 395–401.
- Patrick, R.A.D., Mosselmans, J.F.W., Charnock, J.M., England, K.E.R., Helz, G.R., Garner, C.D., Vaughan, D.J., 1997. The structure of amorphous copper sulfide precipitates: an X-ray absorption study. *Geochim. Cosmochim. Acta* **61**, 2023–2036.
- Pecharrmán, C., González-Carreño, T., Inglesias, J.E., 1995. The infrared dielectric properties of maghemite,  $\gamma$ -Fe<sub>2</sub>O<sub>3</sub>, from reflectance measurement on pressed powders. *Phys. Chem. Miner.* **22**, 21–29.
- Perry, D.L., Taylor, J.A., 1986. X-ray photoelectron and Auger spectroscopic studies of Cu<sub>2</sub>S and CuS. *J. Mater. Sci. Lett.* **5**, 384–386.
- Petiau, J., Sainctavit, Ph., Calas, G., 1988. K X-ray absorption spectra and electronic structure of chalcopyrite CuFeS<sub>2</sub>. *Mater. Sci. Eng. B* **1**, 237–249.
- Powell, A.V., Vaqueiro, P., Knight, K.S., Chapon, L.C., Sánchez, R.D., 2004. Structure and magnetism in synthetic pyrrhotite Fe<sub>7</sub>S<sub>8</sub>: a powder neutron-diffraction study. *Phys. Rev. B* **70**, 014415-1–014415-12.
- Ravel, B., 2001. ATOMS: crystallography for the X-ray absorption spectroscopist. *J. Synchrotron Rad.* **8**, 314–316.
- Rupp, H., Weser, U., 1976. X-ray photoelectron spectroscopy of copper(II), copper(I), and mixed valence systems. *Bioinorg. Chem.* **6**, 45–59.
- Schedel-Niedrig, T., Neisius, T., Böttger, I., Kitzelmann, E., Weinberg, G., Demuth, D., Schlögl, R., 2000. Copper (sub)oxide formation: a surface sensitive characterization of model catalysts. *Phys. Chem. Chem. Phys.* **2**, 2407–2417.
- Schmidt, O., Fazan, T.A., Morais, J., Fecher, G.H., 2001. Microanalysis of the surface of natural iron-based minerals by means of synchrotron radiation based experimental techniques. *Surf. Sci.* **482–485**, 568–573.
- Schwarz, K., Blaha, P., Madsen, G.K.H., 2002. Electronic structure calculations of solids using the WIEN2k package for material sciences. *Comput. Phys. Commun.* **147**, 71–76.
- Skála, R., Cisarová, I., 2005. Crystal structure of troilite from chondrites Eter and Georgetown. *Proc. Lunar Planet. Sci.* **XXXVI**, 1284.
- Skinner, W.M., Nesbitt, H.W., Pratt, A.R., 2004. XPS identification of bulk hole defects and itinerant Fe 3d electrons in natural troilite (FeS). *Geochim. Cosmochim. Acta* **68**, 2259–2263.
- Soriano, L., Abbate, M., de Groot, F.M.F., Alders, D., Fuggle, J.C., Hofmann, S., Petersen, H., Braun, W., 1993. Chemical analysis of passivated and oxidized layers on FeCr and FeTi alloys by soft X-ray absorption spectroscopy. *Surf. Interface Anal.* **20**, 21–26.
- Suga, S., Kimura, A., Matsushita, T., Sekiyama, A., Imada, S., Mamiya, K., Fujimori, A., Takahashi, H., Mori, N., 1999. 2p resonance photoemission and Auger features in NiS<sub>2</sub> and FeS<sub>2</sub>. *Phys. Rev. B* **60**, 5049–5054.
- Sugiura, C., 1981. Sulfur K X-ray absorption spectra of FeS, FeS<sub>2</sub>, and Fe<sub>2</sub>S<sub>3</sub>. *J. Chem. Phys.* **74**, 215–217.
- Todd, E.C., Sherman, D.M., 2003. Surface oxidation of chalcocite (Cu<sub>2</sub>S) under aqueous (pH = 2–11) and ambient atmospheric conditions: mineralogy from Cu L- and O K-edge X-ray absorption spectroscopy. *Am. Miner.* **88**, 1652–1656.
- Todd, E., Sherman, D.M., Purton, J.A., 2000. Nature of sulphide mineral surfaces under atmospheric conditions: results from NEXAFS. *J. Conf. Abstr.* **5**, 1010.
- Todd, E.C., Sherman, D.M., Purton, J.A., 2003a. Surface oxidation of pyrite under ambient atmospheric and aqueous (pH = 2 to 10) conditions: electronic structure and mineralogy from X-ray absorption spectroscopy. *Geochim. Cosmochim. Acta* **67**, 881–893.
- Todd, E.C., Sherman, D.M., Purton, J.A., 2003b. Surface oxidation of chalcopyrite (CuFeS<sub>2</sub>) under ambient atmospheric and aqueous (pH 2–10) conditions: Cu, Fe L- and O K-edge X-ray spectroscopy. *Geochim. Cosmochim. Acta* **67**, 2137–2146.
- Tossell, J.A., Urch, D.S., Vaughan, D.J., Wiech, G., 1982. The electronic structure of CuFeS<sub>2</sub>, chalcopyrite, from X-ray emission and X-ray photoelectron spectroscopy and  $X\alpha$  calculations. *J. Chem. Phys.* **77**, 77–82.

- Ueda, H., Nohara, M., Kitazawa, K., Takagi, H., Fujimori, A., Mizokawa, T., Yagi, T., 2002. Copper pyrites  $\text{CuS}_2$  and  $\text{CuSe}_2$  as anion conductors. *Phys. Rev. B* **65**, 155104-1–155104-5.
- van Aken, P.A., Liebscher, B., 2002. Quantification of ferrous/ferric ratios in minerals: new evaluation schemes of Fe  $L_{2,3}$  electron energy-loss near-edge spectra. *Phys. Chem. Miner.* **29**, 188–200.
- van der Laan, G., Patrick, R.A.D., Charnock, J.M., Grguric, B.A., 2002. Cu  $L_{2,3}$  X-ray absorption and the electronic structure of nonstoichiometric  $\text{Cu}_5\text{FeS}_4$ . *Phys. Rev. B* **66**, 045104-1–045104-5.
- van der Laan, G., Patrick, R.A.D., Henderson, C.M.B., Vaughan, D.J., 1992. Oxidation state variations in copper minerals studied with Cu 2p X-ray absorption spectroscopy. *J. Phys. Chem. Solids* **53**, 1185–1190.
- Vaughan, D.J., Craig, J.R., 1978. *Mineral Chemistry of Metal Sulfides*. Cambridge University Press, Cambridge.
- von Oertzen, G.U., Jones, R.T., Gerson, A.R., 2005. Electronic and optical properties of Fe, Zn and Pb sulfides. *J. Electron Spectrosc.* **144–147**, 1245–1247.
- Yamaguchi, S., Wada, H., 1973. Magnetic iron sulfide of the  $\gamma\text{-Al}_2\text{O}_3$  type. *J. Appl. Phys.* **44**, 1929.
- Zheng, F., Pérez-Dieste, V., McChesney, J.L., Luk, Y.-Y., Abbott, N.L., Himpsel, F.J., 2005. Detection and switching of the oxidation state of Fe in a self-assembled monolayer. *Surf. Sci.* **587**, L191–L196.